Nonlinear effects in optical pumping of atoms by a high-intensity multimode gas laser. II. Exact theory for small angular momenta

Martial Ducloy

Laboratoire de Spectroscopie Hertzienne de l'Ecole, Normale Supérieure, Associé au Centre National de la Recherche, Scientifique, 75231 Paris Cedex 05, France

(Received 22 August 1973)

In a previous paper, I have presented a general theory of the optical pumping of atoms by a polarized multimode-laser beam, in the presence of a magnetic field. Equations of motion, valid at arbitrary laser intensities for the density matrix of the atomic system, have been obtained. In this paper, these equations are exactly solved for a linearly σ-polarized laser and levels having small angular momenta. More precisely, I consider the laser transitions $J_b=1 \rightarrow J_a=0$, $J_b=1 \rightarrow J_a=1$, and $J_b=1 \rightarrow J_a=2$. Two particular results are emphasized: (i) For $J=1$-$J=0$ and $J=1$-$J=1$ transitions and for the $J=2$ level of a $J=1$-$J=2$ transition, the *laser-induced Hanle effects* keep a Lorentzian shape, independent of the laser intensity. For the $J=1$-$J=1$ transition, it is shown that the depolarizing relaxation processes play a leading part in the coupling induced by the laser between the transverse alignments of the two levels. On the other hand, the power broadenings of the Hanle effects are shown to be similar. For the $J=1$ level of a $J=1$-$J=2$ transition, the Hanle-effect shape presents a departure from the Lorentzian one, owing to a coupling with the laser-induced hexadecapole moment in the $J=2$ level. (ii) The populations of the levels exhibit a "*zero-field saturation resonance*" which is due to the coupling with the Zeeman coherences. These resonances, which reproduce the Hanle effects of the transition, can be observed on the π-polarized fluorescence from the levels. In general, these resonances appear as a saturation effect, i.e., they reduce the laser-induced fluorescence of the levels in zero magnetic field. However, for the $J_b=1 \rightarrow J_a=2$ transition, the $J_a=2 \rightarrow J_f=2$ π fluorescence presents an anomalous behavior; the saturation resonance increases the zero-field laser-induced fluorescence. The theoretical study shows the prominent part played by the value of the $J_b=1$ level lifetime in the interpretation of this anomaly. Other results, such as the laser-induced depolarization of the fluorescence, are also obtained. All the theoretical predictions have been experimentally checked and will be presented in forthcoming papers.

I. INTRODUCTION

In a previous paper,[1] which will be referred to as I in the following, I have presented a general theory of the optical pumping of atoms by a multimode gas laser. Let us recall the principal assumptions.

The laser is resonant for the b-a atomic transition (b upper level, a lower level). Every level has a Zeeman structure completely determined by its angular momentum J_β and its Landé factor $g_\beta(\beta=a \text{ or } b)$. The atomic levels are populated by a dc discharge which introduces a global population only. The atoms are submitted to a dc magnetic field H, parallel to the $0z$ axis. They are described by means of their density matrix ${}_\beta\rho$ which is developed on an irreducible tensorial set;

$$ {}_\beta\rho = \sum_{k,Q} {}_\beta\rho^k_Q \, {}_\beta T^{(k)}_Q . \tag{1} $$

The atomic relaxation is assumed to be isotropic; there is one relaxation rate $\Gamma_\beta(k)$ per tensorial order.

In order to avoid the usual perturbation theory, we have introduced in I the so-called "broad-line approximation" (BLA). BLA is valid when the width of the "Bennett hole"[2] created by one laser mode in the velocity distribution of the excited atoms is comparable to (or broader than) the spacing between modes; in these conditions, *the atomic response does not depend on the velocity*, and the multimode-laser irradiation is equivalent to a broad-line excitation. BLA leads to a set of equations coupling the velocity-averaged density-matrix components and valid at arbitrary intensities of the laser field. These equations depend on the electric field through an unique parameter γ which is proportional to the laser intensity and which can be interpreted as a laser-induced transition probability [Eq.(I-46)].

In I, I have analyzed the nonlinear effects which can be deduced from a perturbation development for *any* values of the angular momenta, of the magnetic field, and of the laser polarization. In this article, I present the exact calculations for a linear σ polarization (that we shall take parallel to $0x$)

and for small J values; more precisely, I completely calculate the nonlinear effects for the following transitions: 1-0, 1-1, and 1-2.

Moreover, condition (I-68) ($\Gamma_\beta \ll \Delta\omega$) is assumed to be valid, and I consider the case of weak magnetic fields only, when the density-matrix modulations are off resonance. Then, in the steady-state operation, Eqs. (I-50) and (I-51) are reduced to a set of equations coupling the time-independent components ($\beta = a$ or b):

$$(\Gamma_\beta(k) + iQ\omega_\beta)\,{}_\beta\rho_Q^k = \delta_{\beta,a}\Theta(b,a,k)\,{}_b\rho_Q^k + {}_\beta\zeta_Q^k, \quad (2)$$

where

$${}_a\zeta_Q^k = -\gamma \sum_{k'Q'q} (-)^{k+k'}\,{}^q_{ab}G^{k'k}_{Q'Q}\left[e_{-q}\,{}_{ab}\zeta^{k'}_{Q'} + (-)^{k+k'+Q+1} e^*_q\,{}_{ab}\zeta^{k'*}_{-Q'}\right], \quad (3a)$$

$${}_b\zeta_Q^k = -\gamma \sum_{k'Q'q} {}^q_{ba}G^{k'k}_{Q'Q}\left[e_{-q}\,{}_{ab}\zeta^{k'}_{Q'} + (-)^{k+k'+Q+1} e^*_q\,{}_{ab}\zeta^{k'*}_{-Q'}\right], \quad (3b)$$

and

$${}_{ab}\zeta^{k'}_{Q'} = e^*_{Q'}\frac{n}{\sqrt{3}}\,\delta_{k'1} + \sum_{k''Q''q'} e^*_{-q'}\left[{}^{q'}_{ba}G^{k'k''}_{Q'Q''}\,{}_b\rho^{k''}_{Q''} + (-)^{k'+k''}\,{}^{q'}_{ab}G^{k'k''}_{Q'Q''}\,{}_a\rho^{k''}_{Q''}\right]. \quad (4)$$

The geometrical coefficients G and Θ are defined by (I-19) and (I-21). n is the laser-off populations inversion (I-24). ω_β is the β Zeeman splitting, and e_q are the standard components of the laser polarization. Let us remember that (a) ρ *represents the laser-induced change of the density matrix* (the laser-off populations have been eliminated), and (b) ${}_{ab}\zeta^{k'}_{Q'}$ appeared in the source term of the equation of motion of the optical coherence ${}_{ab}\rho^{k'}_{Q'}$ [see (I-28)]. ${}_{ab}\zeta^{k'}_{Q'}$ *is proportional to the amplitude of the optical k'-multipole moment created by the laser between a and b.*

When the laser modes are free running, Eqs. (2)–(4) are valid whatever the magnetic field may be. On the other hand, when the modes are phase locked and when the Landé factors are equal, the results obtained in this paper may be easily extended to the strong fields case, with the help of equations (I-83) and (I-84). By solving Eqs. (2)–(4), we shall study the quantities which can be obtained in fluorescence measurements, in particular the following: (1) *The density-matrix components in zero magnetic field.* They appear in the anisotropy degree of the zero-field fluorescence [the exact definition of this anisotropy is given in Sec. E of Ref. 3, in particular, Eq. (68)]. (2) *The transverse alignments* ρ_2^2. The variations of their real part with the magnetic field give the Hanle effect. (3) *The longitudinal components* (i.e., the populations of the sublevels) which are observable on the π-polarized fluorescence.

II. GENERAL WAY OF SOLVING THE EQUATIONS OF MOTION

In order to solve the equations of motion, it is important to point out that the density-matrix components do not represent a set of independent variables. For instance, linear relations exist between the longitudinal components ${}_\beta\rho^k_0$. The most simple relation may be deduced from the fact that ${}_b\zeta^0_0(2J_b+1)^{1/2} = -{}_a\zeta^0_0(2J_a+1)^{1/2}$. This implies

$$\left[\Gamma_b(0) - \gamma_{ba}\right]{}_b\rho^0_0(2J_b+1)^{1/2} + \Gamma_a(0)\,{}_a\rho^0_0(2J_a+1)^{1/2} = 0. \quad (5)$$

Since the laser-induced population change of the β level is ${}_\beta\rho^0_0(2J_\beta+1)^{1/2}$, (5) expresses the conservation of the total population inside the a and b levels: All the atoms leaving one of the two levels due to the laser interaction must go into the other level. The γ_{ba} term takes into account the excitation rate of the a level by spontaneous emission from b. The other relations between the longitudinal components could be deduced from a detailed analysis of the laser-induced exchange rate of the sublevel populations for each set of Zeeman sublevels coupled by the laser.

We shall see that, contrary to ${}_\beta\rho^k_Q$, the ${}_{ab}\zeta^{k'}_{Q'}$ components represent a set of independent variables [i.e., they are not coupled by simple linear relations similar to Eq. (5)]. That is the reason why these components have been kept in (2) and (3): They will be an important intermediate step in the search of the solution.

A. Zero magnetic field

Taking the $0z$ axis along the laser polarization, we can set $Q = Q' = Q'' = 0$ in (2)–(4). On the other hand, as it has been shown in I, k' must be odd, and k and k'' must be even. If we call σ the density matrix such as expressed in this quantization axis, Eqs. (3) and (4) become

$$\Gamma_\beta(k)\,{}_\beta\sigma^k_0 = \delta_{\beta,a}\Theta(b,a,k)\,{}_b\sigma^k_0 + {}_\beta\zeta^k_0, \quad (6)$$

$${}_a\zeta^k_0 = 2\gamma \sum_{k'} {}^0_{ab}G^{k'k}_{00}\,{}_{ab}\zeta^{k'}_0, \quad (7a)$$

$${}_b\zeta^k_0 = -2\gamma \sum_{k'} {}^0_{ba}G^{k'k}_{00}\,{}_{ab}\zeta^{k'}_0, \quad (7b)$$

and

$$ {}_{ab}\zeta_0^{k'} = \frac{n}{\sqrt{3}}\,\delta_{k'1} + \sum_{k''} \left({}^{0}_{ba}G^{k'k''}_{00}\,{}_{b}\sigma_0^{k''} - {}^{0}_{ab}G^{k'k''}_{00}\,{}_{a}\sigma_0^{k''} \right). \tag{8} $$

Eliminating ${}_{\beta}\sigma$ between Eqs. (6)–(8), we easily obtain

$$ \sum_{l'} M_0^{k'l'}\,{}_{ab}\zeta_0^{l'} = \frac{n}{\sqrt{3}}\,\delta_{k'1}, \tag{9} $$

where

$$ M_0^{k'l'} = \delta_{k'l'} + 2\gamma \sum_{k} \left(\frac{{}^{0}_{ba}G^{k'k}_{00}\,{}^{0}_{ba}G^{l'k}_{00}}{\Gamma_b(k)} + \frac{{}^{0}_{ab}G^{k'k}_{00}\,{}^{0}_{ab}G^{l'k}_{00}}{\Gamma_a(k)} - \Theta(b,a,k)\,\frac{{}^{0}_{ab}G^{k'k}_{00}\,{}^{0}_{ba}G^{l'k}_{00}}{\Gamma_b(k)\Gamma_a(k)} \right). \tag{10} $$

The solution is obtained by inversing matrix M_0.[4] As it has been mentioned in I, for $J=1$-$J=0$ and $J=1$-$J=1$ transitions, k' can be 1 only, and M_0 has an unique matrix element M_0^{11}. In these cases, all the density-matrix components are proportional to $\gamma\,{}_{ab}\zeta_0^1$ and show the same variations with the laser intensity. For a $J=1$-$J=2$ transition ${}_{ab}\zeta_0^3$ exists in addition to ${}_{ab}\zeta_0^1$, and M_0 is a 2×2 matrix. The various density-matrix components do not undergo identical variations with the laser intensity. To come back to our ordinary framework (laser polarized along the $0x$ axis), we must perform the rotation which brings $0z$ on $0x$. The transformation formulas are[5]

$$ \rho_Q^k(H=0) = (-)^{(k+Q)/2}\,\frac{[(k+Q)!\,(k-Q)!\,]^{1/2}}{2^k[(k+Q)/2]!\,[(k-Q)/2]!}\,\sigma_0^k. \tag{11} $$

B. Nonzero magnetic field

The standard components of a σ_x polarization are given by

$$ e_0 = 0 \quad \text{and} \quad e_{\pm 1} = \mp 1/\sqrt{2}. \tag{12} $$

As it has been shown in I, owing to the symmetry relations of the G coefficients and to (12), k, k'', Q, and Q'' must be even in (2)–(4). On the other hand, for the optical coherences, Q' must be odd, and k' may take all the integer values between 1 and $J_a + J_b$. Then, it is easy to show the following symmetry relation:

$$ {}_{ab}\zeta^{k'*}_{-Q'} = (-)^{k'}\,{}_{ab}\zeta^{k'}_{Q'}. \tag{13} $$

With the help of (12) and (13), Eqs. (3) and (4) become

$$ {}_{a}\zeta_Q^k = \gamma\sqrt{2}\sum_{k'} (-)^{k'} \left({}^{-1}_{ab}G^{k'k}_{Q+1,\,Q}\,{}_{ab}\zeta^{k'}_{Q+1} - {}^{1}_{ab}G^{k'k}_{Q-1,\,Q}\,{}_{ab}\zeta^{k'}_{Q-1} \right), \tag{14} $$

$$ {}_{b}\zeta_Q^k = \gamma\sqrt{2}\sum_{k'} \left({}^{-1}_{ba}G^{k'k}_{Q+1,\,Q}\,{}_{ab}\zeta^{k'}_{Q+1} - {}^{1}_{ba}G^{k'k}_{Q-1,\,Q}\,{}_{ab}\zeta^{k'}_{Q-1} \right), \tag{15} $$

and

$$ {}_{ab}\zeta^{k'}_{Q'} = \frac{n}{\sqrt{6}}\,\delta_{k',1}(\delta_{Q',-1} - \delta_{Q',1}) + \frac{(-)^{k'}}{\sqrt{2}}\sum_{k''} \left({}^{1}_{ab}G^{k'k''}_{Q',Q'+1}\,{}_{a}\rho^{k''}_{Q'+1} - {}^{-1}_{ab}G^{k'k''}_{Q',Q'-1}\,{}_{a}\rho^{k''}_{Q'-1} \right) + \frac{1}{\sqrt{2}}\sum_{k''} \left({}^{1}_{ba}G^{k'k''}_{Q',Q'+1}\,{}_{b}\rho^{k''}_{Q'+1} - {}^{-1}_{ba}G^{k'k''}_{Q',Q'-1}\,{}_{b}\rho^{k''}_{Q'-1} \right). \tag{16} $$

To solve Eqs. (2) and (14)–(16), we shall eliminate first the longitudinal components, which do not precess in the magnetic field, in order to obtain a set of equations only coupling the transverse components which describe the evolution of the Zeeman coherence owing to the magnetic field.

1. *Elimination of the longitudinal components*

Using the symmetry relations of coefficients G and introducing a quantity proportional to the real part of ${}_{ab}\zeta_1^{k'}$,

$$ X^{k'} = \frac{(-)^{k'+1}}{\sqrt{2}} \left({}_{ab}\zeta_1^{k'} + {}_{ab}\zeta_1^{k'*} \right), \tag{17} $$

Eqs. (2) and (14)–(16) become (for $Q=0$ and $Q'=1$)

$$ \Gamma_a(k)\,{}_{a}\rho_0^k = 2\gamma \sum_{k'} \left((-)^{k'}\,{}^{1}_{ab}G^{k'k}_{-10} + \frac{\Theta(b,a,k)}{\Gamma_b(k)}\,{}^{1}_{ba}G^{k'k}_{-10} \right) X^{k'}, \tag{18a} $$

$$ \Gamma_b(k)\,{}_{b}\rho_0^k = 2\gamma \sum_{k'} {}^{1}_{ba}G^{k'k}_{-10} X^{k'}, \tag{18b} $$

and

$$ X^{k'} = -\frac{n}{\sqrt{3}}\,\delta_{k'1} - \sum_{k''} \left[{}^{1}_{ba}G^{k'k''}_{-10}\,{}_{b}\rho_0^{k''} + (-)^{k'}\,{}^{1}_{ab}G^{k'k''}_{-10}\,{}_{a}\rho_0^{k''} \right] - \sum_{k''} \left[(-)^{k'}\,{}^{1}_{ba}G^{k'k''}_{12}\,{}_{b}R_2^{k''} + {}^{1}_{ab}G^{k'k''}_{12}\,{}_{a}R_2^{k''} \right], \tag{19} $$

where R_Q^k is the real part of ρ_Q^k;

$$ {}_{\beta}R_Q^k = \tfrac{1}{2}\left({}_{\beta}\rho_Q^k + {}_{\beta}\rho_Q^{k*} \right). \tag{20} $$

Eliminating ${}_{\beta}\rho_0^k$ between Eqs. (18) and (19), we obtain

$$ \sum_{l'} M^{k'l'}X^{l'} = -\frac{n}{\sqrt{3}}\,\delta_{k'1} - \sum_{k''} \left[(-)^{k'}\,{}^{1}_{ba}G^{k'k''}_{12}\,{}_{b}R_2^{k''} + {}^{1}_{ab}G^{k'k''}_{12}\,{}_{a}R_2^{k''} \right], \tag{21} $$

where

$$M^{k'l'}=\delta_{k'l'}+2\gamma\sum_k\left(\frac{{}^1_{ba}G^{k'k}_{-10}\,{}^1_{ba}G^{l'k}_{-10}}{\Gamma_b(k)}+(-)^{k'+l'}\frac{{}^1_{ab}G^{k'k}_{-10}\,{}^1_{ab}G^{l'k}_{-10}}{\Gamma_a(k)}+(-)^{k'}\Theta(b,a,k)\frac{{}^1_{ab}G^{k'k}_{-10}\,{}^1_{ba}G^{l'k}_{-10}}{\Gamma_a(k)\Gamma_b(k)}\right). \tag{22}$$

M is a square matrix of dimension J_a+J_b. As M_0, M is symmetrical when the $b\to a$ spontaneous emission is negligible. We suppose that we can calculate its inverse matrix, and we call it μ/Δ, where Δ is the determinant of M. Then, the solution of (21) is

$$X^{k'}=-\frac{n}{\sqrt{3}}\frac{\mu^{k'1}}{\Delta}-\frac{1}{\Delta}\sum_{l'',k''}\mu^{k'l''}[(-)^{l''}\,{}^1_{ba}G^{l''k''}_{12}\,{}_bR^{k''}_2+{}^1_{ab}G^{l''k''}_{12}\,{}_aR^{k''}_2]. \tag{23}$$

Δ and $\mu^{k'l'}$, taken as functions of γ, are polynomials of degrees respectively equal to J_a+J_b and J_a+J_b-1.

2. *Equations of motion of the transverse components: Hanle effects*

Using (2), (14)–(16), and the relation

$$(-)^{k'}\sqrt{2}\,{}_{ab}\xi^{k'}_1+X^{k'}=\sum_{k''}[(-)^{k'}\,{}^1_{ba}G^{k'k''}_{12}({}_b\rho^{k''}_2-{}_bR^{k''}_2)+{}^1_{ab}G^{k'k''}_{12}({}_a\rho^{k''}_2-{}_aR^{k''}_2)], \tag{24}$$

we obtain the following equations of motion for ${}_b\rho^k_2$:

$$[\Gamma_b(k)+2i\omega_b]\,{}_b\rho^k_2=\gamma\sum_{k'',Q''\geq 2}({}_{ba}h^{kk''}_{2Q''}\,{}_a\rho^{k''}_{Q''}-{}_bh^{kk''}_{2Q''}\,{}_b\rho^{k''}_{Q''})$$
$$+\gamma\sum_{k'}(-)^{k'}\,{}^1_{ba}G^{k'k}_{12}\left(X^{k'}+\sum_{k''}[(-)^{k'}\,{}^1_{ba}G^{k'k''}_{12}\,{}_bR^{k''}_2+{}^1_{ab}G^{k'k''}_{12}\,{}_aR^{k''}_2]\right). \tag{25}$$

To simplify the formulation, we have reintroduced the geometrical coefficients $h^{kk''}_{QQ''}$, which are defined by Eqs. (I-62) and (I-63). In the right-hand side of (25), two different contributions appear: The first contribution corresponds to the *direct* laser-induced coupling between the *transverse* components. This coupling is proportional to γ. The second term corresponds to an *indirect* coupling between the $Q=2$ transverse components through the *longitudinal* quantities. Since these quantities are real, this coupling involves the real part of the transverse components only. The second term also includes the source term, proportional to the laser-off population inversion n.

For the a level, the coupling by spontaneous emission from b to a must be added to these two contributions. For $Q\geq 4$, ${}_\beta\rho^k_Q$ is not directly coupled to the longitudinal components, and the second term of (25) does not appear. The equations of motion are

$$[\Gamma_b(k)+iQ\omega_b]\,{}_b\rho^k_Q=\gamma\sum_{k'',Q''}({}_{ba}h^{kk''}_{QQ''}\,{}_a\rho^{k''}_{Q''}-{}_bh^{kk''}_{QQ''}\,{}_b\rho^{k''}_{Q''}) \tag{26}$$

(and similar equations for level a).

To obtain the expression of the transverse components, Eqs. (25) and (26) must be solved simultaneously. For the $J=1$-$J=0$ and $J=1$-$J=1$ transitions, the transverse alignments are the only transverse components. In this case, Eq. (26) does not exist, and Eqs. (25) are reduced to one (1-0) or two (1-1) equations. We shall see that an analytic solution may be obtained. For the $J_b=1\to J_a=2$ transition, there are three Eqs. (25) (${}_a\rho^2_2$, ${}_a\rho^4_2$, and ${}_b\rho^2_2$) and one Eq. (26) (${}_a\rho^4_4$). The only way to solve these equations, for all the magnetic field values, is by means of a computer calculation.

The variations of the transverse components with the magnetic field give the well-known Hanle effects. In the following, we shall use the notation (for $Q\neq 0$)

$${}_\beta R^k_Q(H)={}_\beta R^k_Q(0)\;{}_\beta L^k_Q(H). \tag{27}$$

In zero magnetic field, ${}_\beta L^k_Q(0)$ is equal to 1, and, in strong fields, ${}_\beta L^k_Q(\infty)$ vanishes. ${}_\beta L^k_Q(H)$ represents the "*normalized Hanle effect.*" On the other hand, since $R^k_Q(0)$ is defined in zero field, we may calculate it by means of Eqs. (6)–(11).

3. *"Saturation resonances" of the sublevels populations*

When the transverse components have been calculated, the longitudinal ones may be expressed by means of (18) and (23). The longitudinal components, i.e., the populations of the atomic sublevels, exhibit variations in the zero magnetic field region which are proportional to ${}_\beta R^k_2(H)$. These variations, which appear from the fourth order in the laser

field only, will be called "saturation resonances." Let me point out that it is not necessary to solve (25) and (26) to obtain the relative amplitude of the saturation resonance. As it can be seen in Eqs. (18) and (23), it is sufficient to determine the μ matrix and to calculate the zero-field components ${}_{\beta}R_2^k(0)$. For instance, the amplitude of the saturation resonance on level b is given by

$$\frac{{}_b\rho_0^k(\infty)-{}_b\rho_0^k(0)}{{}_b\rho_0^k(\infty)}=-\frac{\sqrt{3}\sum_{k'l'k''}{}_{ba}^{1}G_{-10}^{k'k}\mu^{k'l''}[(-)^{l''}{}_{ba}^{1}G_{12}^{l'k''}\,{}_bR_2^{k''}(0)+{}_{ab}^{1}G_{12}^{l'k''}\,{}_aR_2^{k''}(0)]}{n\sum_{k'}{}_{ba}^{1}G_{-10}^{k'k}\mu^{k'1}}\,. \tag{28}$$

C. Conclusion

In Sec. II, we have presented the way of solving the equations of motion. In Secs. III–V this will be applied to $J=1\text{-}J=0$, $J=1\text{-}J=1$, and $J=1\text{-}J=2$ transitions, respectively. For each case, the geometrical coefficients ${}_{\beta\alpha}^{q}G_{QQ}^{kk'}$, and $\Theta(b,a,k)$ [Eqs. (I-19) and (I-21)] will be calculated using the numerical values of the 3-j and 6-j symbols which may be found in tables.[6,7] Numerical applications of the theory to the laser experiments in neon will be performed with the help of the experimental values of the relaxation times of the neon levels.[8-10]

III. TRANSITION $J_b=1\rightarrow J_a=0$

For a 1-0 transition, the optical coherence is reduced to the electric dipole moment ($k'=1$). Then, as it can be seen in Eq. (18), all the longitudinal components of the density matrix are proportional, independent of the laser intensity and of the magnetic field;

$$-\Gamma_a^*(0)\,{}_a\rho_0^0=\sqrt{3}\Gamma_b(0)\,{}_b\rho_0^0=\sqrt{6}\Gamma_b(2)\,{}_b\rho_0^2=(2\gamma/\sqrt{3})X^1\,, \tag{29}$$

where

$$\Gamma_a^*(0)=\Gamma_a(0)[1-\gamma_{ba}/\Gamma_b(0)]^{-1}\,. \tag{30}$$

As it has been pointed out in Sec. II, the relation between ${}_b\rho_0^0$ and ${}_a\rho_0^0$ expresses the conservation of the total population during a laser-induced transition between levels a and b. On the other hand, the proportionality between the population and the alignment of b comes from the fact that the $m_b=1$ and $m_b=-1$ sublevels are equally excited by the laser, while the $m_b=0$ sublevel is populated by the depolarizing relaxation processes only. For instance, if these processes do not exist [$\Gamma_b(0)=\Gamma_b(2)$], relation ${}_b\rho_0^0=\sqrt{2}\,{}_b\rho_0^2$ may be easily obtained from the fact that there is no laser-induced change of the $m=0$ population.

Matrix M [Eq. (22)] is reduced to one element;

$$M^{11}=1+\eta\gamma/3\Gamma_b(2)\,, \tag{31}$$

where we have introduced a dimensionless parameter

$$\eta=\tfrac{1}{3}+2\Gamma_b(2)/3\Gamma_b(0)+2\Gamma_b(2)/\Gamma_a^*(0)\,. \tag{32}$$

X^1 is given by [Eq. (21)]

$$M^{11}X^1=-(n-{}_bR_2^2)/\sqrt{3}\,. \tag{33}$$

A. Hanle effect of the b level

The equation of motion of the transverse alignment is given by [Eqs. (25) and (33)]

$$[\Gamma_b(2)+2i\omega_b]\,{}_b\rho_2^2=-\frac{\gamma}{3}\,{}_b\rho_2^2+\frac{\gamma}{3+\eta\gamma/\Gamma_b(2)}\left(n+\eta\,\frac{\gamma}{3\Gamma_b(2)}\,{}_bR_2^2\right). \tag{34}$$

${}_b\rho_2^2$ is calculated with the help of Eq. (34) and its complex conjugate;

$${}_b\rho_2^2(H)=\frac{n\gamma}{3+\eta\gamma/\Gamma_b(2)}\,\frac{\Gamma_b(2)+\frac{1}{3}\gamma-2i\omega_b}{[\gamma_b'(2)]^2+4\omega_b^2}\,, \tag{35}$$

where

$$\gamma_b'(2)=\Gamma_b(2)\times\left\{\frac{[1+\gamma/3\Gamma_b(2)][1+(\eta+1)\gamma/3\Gamma_b(2)]}{1+\eta\gamma/3\Gamma_b(2)}\right\}^{1/2}. \tag{36}$$

The Hanle effect, which is described by the variations of ${}_bR_2^2$ with ω_b, always keeps a Lorentzian shape, independently of the laser intensity. This has been experimentally verified very well.[11] The variations of its width with the pumping rate γ are shown on Fig. 1 for $\eta=4.75$ and $\Gamma_b(2)=11$ MHz. For weak laser intensities, the power broadening, which is equal to $\frac{1}{3}\gamma$ [first term in the right-hand side of (34)], is proportional to the laser-induced transition probability. This corresponds to the fourth-order contribution in a perturbation development [see Eq. (I-77)]. For strong laser intensities, the power broadening becomes lower than $\frac{1}{3}\gamma$. Since ${}_bR_2^2$ is equal to $\frac{1}{2}({}_b\rho_2^2+{}_b\rho_{-2}^2)$, the ${}_bR_2^2$ term in Eq. (34) implies a restitution of a part of the Zeeman coherence. This restitution through the longitudinal components appears from the sixth order in the laser field and involves a diminution of the alignment relaxation rate compared with the fourth-order relaxation rate.

The ${}_bR_2^2$ term of (34) also implies a coupling between ρ_2^2 and ρ_{-2}^2. This laser-induced coupling of

${}_b\rho_2^2$ with the component precessing in the opposite direction changes the phase of the Zeeman coherence and shifts the frequency of evolution. In the ordinary magnetic resonance, this kind of coupling induces a resonance shift (Bloch-Siegert effect[12]). Here, since ρ_2^2 and ρ_{-2}^2 are both resonant in zero magnetic field, the resonance is not displaced. But the phase shift changes the relative amplitude of the real and imaginary parts of the coherence. In the ordinary Hanle effect, the absorption curve has the same amplitude as the dispersion curve. Here, their ratio is equal to

$$[\Gamma_b(2)+\tfrac{1}{3}\gamma]/\gamma_b^I(2)\,. \tag{37}$$

It becomes higher than one from the sixth order in the laser electric field.

B. Saturation resonance of the populations

The sublevels populations are proportional to X^1 (29). Using (33) and (35), we obtain

$$X^1 = -\frac{n}{M^{11}\sqrt{3}}\,[1-\mathcal{S}\,{}_bL_2^2(H)], \tag{38}$$

where

$$\mathcal{S} = \gamma/[3\Gamma_b(2)+(\eta+1)\gamma] \tag{39}$$

and ${}_bL_2^2$ is the normalized Hanle effect;

$${}_bL_2^2(H) = \{1+[2\omega_b/\gamma_b^I(2)]^2\}^{-1}\,. \tag{40}$$

As it has been experimentally observed,[11] the populations exhibit a resonance which has exactly the same shape as the Hanle effect. The relative amplitude of this resonance, $\mathcal{S}$, is a homographic function of γ.[13] At high laser intensities, $\mathcal{S}$ is equal to $(\eta+1)^{-1}$ (0.17 in the conditions of Fig. 1).

IV. TRANSITION $J_b=1\rightarrow J_a=1$

In this section, we shall use the following quantities which have the dimension of a time:

$$\tau(0) = \frac{1}{\Gamma_b(0)}+\frac{1}{\Gamma_a(0)}-\frac{\gamma_{ba}}{\Gamma_a(0)\Gamma_b(0)} \tag{41}$$

and

$$\tau_1^1 = \frac{1}{\Gamma_b(2)}+\frac{1}{\Gamma_a(2)}+\frac{\gamma_{ba}}{2\Gamma_a(2)\Gamma_b(2)}, \tag{42a}$$

$$\tau_2^2 = \frac{1}{\Gamma_b(2)}+\frac{1}{\Gamma_a(2)}-\frac{\gamma_{ba}}{2\Gamma_a(2)\Gamma_b(2)}, \tag{42b}$$

$$\tau_1^2 = \frac{1}{\Gamma_b(2)}-\frac{1}{\Gamma_a(2)}+\frac{\gamma_{ba}}{2\Gamma_a(2)\Gamma_b(2)}, \tag{42c}$$

$$\tau_2^1 = \frac{1}{\Gamma_b(2)}-\frac{1}{\Gamma_a(2)}-\frac{\gamma_{ba}}{2\Gamma_a(2)\Gamma_b(2)}\,. \tag{42d}$$

These quantities will appear in the matrix elements of M_0 and M.

A. Zero magnetic field

In zero field, the laser creates an optical dipole moment only ($k'=1$). As it has been shown in Sec. II A from Eqs. (6)–(11), all the density-matrix components are proportional to $\gamma_{ab}\zeta_0^1$;

$$\Gamma_b(0)\,{}_b\rho_0^0 = -2\sqrt{2}\,\Gamma_b(2)\,{}_b\rho_0^2 = \frac{4\Gamma_b(2)}{\sqrt{3}}\,{}_b\rho_{\pm 2}^2 = -\frac{2n\gamma}{3M_0^{11}\sqrt{3}}, \tag{43a}$$

$$\Gamma_a^*(k)\,{}_a\rho_Q^k = -\Gamma_b(k)\,{}_b\rho_Q^k, \tag{43b}$$

where

$$M_0^{11} = 1+\tfrac{1}{9}\gamma[2\tau(0)+\tau_1^1]\,. \tag{44}$$

$\Gamma_a^*(0)$ is given by (30) and $\Gamma_a^*(2)$ by

$$\Gamma_a^*(2) = \Gamma_a(2)[1+\gamma_{ba}/2\Gamma_b(2)]^{-1}\,. \tag{45}$$

B. Hanle effects

When the magnetic field is different from zero, the laser may create, in addition to the optical dipole moment, an optical quadrupole moment ($k'=2$), which is connected to the apparition, for high laser intensities, of the quantity X^2 (17). The M matrix (22) has four components:

$$M = \begin{pmatrix} 1+\gamma[\frac{2}{9}\tau(0)+\frac{1}{36}\tau_1^1] & -\frac{1}{12}\gamma\tau_1^2 \\ -\frac{1}{12}\gamma\tau_2^1 & 1+\gamma\frac{1}{4}\tau_2^2 \end{pmatrix}, \tag{46}$$

and its determinant is given by

$$\Delta = 1+\gamma\left(\frac{2\tau(0)}{9}+\frac{\tau_1^1}{36}+\frac{\tau_2^2}{4}\right)+\frac{\gamma^2}{18}\left(\tau(0)\tau_2^2+\frac{1}{2\Gamma_a(2)\Gamma_b(2)}\right). \tag{47}$$

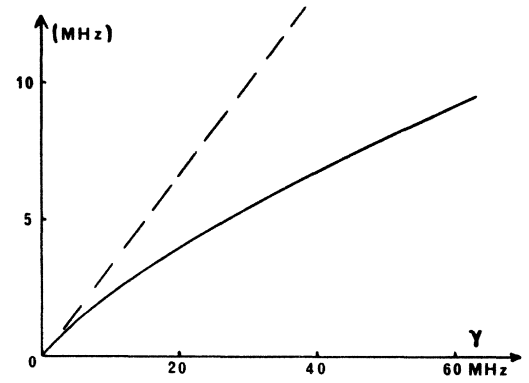

FIG. 1. Power broadening of the b Hanle effect for a $J_b=1$–$J_a=0$ laser transition. Continuous curve: exact power broadening, $\gamma_b^I(2)-\Gamma_b(2)$. Dashed line: fourth-order broadening, $\frac{1}{3}\gamma$. The relaxation rates are, in MHz, $\Gamma_a(0)=9$, $\Gamma_b(0)=3.7$, and $\Gamma_b(2)=11$. This approximately corresponds to 1 torr of neon for the $2s_2$-$2p_1$ neon transition ($\lambda=1.52\ \mu$).

The inversion of M is obvious, and we straightforwardly obtain for $X^{k'}$ [Eq. (23)]

$$X^1 = -\frac{1}{2\Delta\sqrt{3}}\left[\left(1+\gamma\frac{\tau_2^2}{4}\right)(2n+{}_bR_2^2-{}_aR_2^2) + \frac{\gamma\tau_1^2}{12}({}_bR_2^2+{}_aR_2^2)\right], \quad (48a)$$

$$X^2 = -\frac{1}{2\Delta\sqrt{3}}\left[\frac{\gamma\tau_2^1}{12}(2n+{}_bR_2^2-{}_aR_2^2) + \left(1+\gamma\frac{2\tau(0)}{9}+\gamma\frac{\tau_1^1}{36}\right)({}_bR_2^2+{}_aR_2^2)\right]. \quad (48b)$$

In zero magnetic field, ${}_\beta R_2^2$ is equal to ${}_\beta\rho_2^2$ and is given by Eqs. (43). In this case, eliminating ${}_\beta R_2^2$ between (43) and (48b), we may verify that X^2 vanishes, independently of the laser intensity. On the other hand in strong fields, ${}_\beta R_2^2$ vanishes, and X^2 is proportional to τ_2^1. The optical quadrupole moment disappears when $\tau_2^1=0$, i.e., when

$$\Gamma_b(2)=\Gamma_a^*(2). \quad (49)$$

This particular case will be considered in a detailed way later on (Sec. IV D). The equations of motion of the transverse alignments are given by [Eq. 25)]

$$[\Gamma_a(2)+2i\omega_a]\,{}_a\rho_2^2 = -\frac{\gamma_{ba}}{2}{}_b\rho_2^2-\frac{\gamma}{6}{}_a\rho_2^2 + \frac{\gamma}{6}{}_aR_2^2+\frac{\gamma}{2\sqrt{3}}(-X^1+X^2), \quad (50a)$$

$$[\Gamma_b(2)+2i\omega_b]\,{}_b\rho_2^2 = -\frac{\gamma}{6}{}_b\rho_2^2+\frac{\gamma}{6}{}_bR_2^2+\frac{\gamma}{2\sqrt{3}}(X^1+X^2). \quad (50b)$$

As it had been shown in I, there is no direct laser-induced coupling between the transverse alignments [${}_{ba}h_{22}^{22}=0$, see Eq. (I-78)]. Eliminating the imaginary parts of ρ_2^2 between Eqs. (50) and their complex conjugates, and using relations (48), we obtain two coupled equations for ${}_bR_2^2$ and ${}_aR_2^2$:

$$\left(\Gamma_a(2)+\frac{\gamma}{6}\chi_{aa}+\frac{4\omega_a^2}{\Gamma_a(2)+\frac{1}{6}\gamma}\right){}_aR_2^2+\left[\frac{\gamma}{6}\chi_{ba}+\frac{\gamma_{ba}}{2}\left(1-\frac{4\omega_a\omega_b}{[\Gamma_a(2)+\frac{1}{6}\gamma][\Gamma_b(2)+\frac{1}{6}\gamma]}\right)\right]{}_bR_2^2=\frac{n\gamma}{6\Delta}\left[1+\gamma\left(\frac{\tau_2^2}{4}-\frac{\tau_2^1}{12}\right)\right], \quad (51a)$$

$$\frac{\gamma}{6}\chi_{ab}\,{}_aR_2^2+\left(\Gamma_b(2)+\frac{\gamma}{6}\chi_{bb}+\frac{4\omega_b^2}{\Gamma_b(2)+\frac{1}{6}\gamma}\right){}_bR_2^2=-\frac{n\gamma}{6\Delta}\left[1+\gamma\left(\frac{\tau_2^2}{4}+\frac{\tau_2^1}{12}\right)\right], \quad (51b)$$

where

$$\chi_{aa}=\frac{1}{\Delta}\left[1+\frac{\gamma}{9}\left(\tau(0)+\frac{1}{2\Gamma_b(2)}+\frac{2}{\Gamma_a(2)}-\frac{\gamma_{ba}}{2\Gamma_a(2)\Gamma_b(2)}\right)\right], \quad (52a)$$

$$\chi_{ab}=\frac{\gamma}{9\Delta}\left(\tau(0)-\frac{1}{\Gamma_b(2)}-\frac{1}{\Gamma_a(2)}+\frac{\gamma_{ba}}{\Gamma_a(2)\Gamma_b(2)}\right), \quad (52b)$$

$$\chi_{ba}=\frac{\gamma}{9\Delta}\left(\tau(0)-\frac{1}{\Gamma_b(2)}-\frac{1}{\Gamma_a(2)}+\frac{\gamma_{ba}}{4\Gamma_a(2)\Gamma_b(2)}\right). \quad (52c)$$

χ_{bb} is obtained from χ_{aa} by permuting a and b.

In Eqs. (51), there are two different couplings between the alignments: (i) the coupling induced by the $b\to a$ spontaneous emission [γ_{ba} term in (51a)] and (ii) the laser-induced coupling ($\gamma\chi_{ba}$ and $\gamma\chi_{ab}$ terms). Since $\Gamma_\beta(2)$ is larger than $\Gamma_\beta(0)$, Eqs. (52) show that generally χ_{ba} and χ_{ab} are positive. The only way for χ_{ab} and χ_{ba} to be cancelled out is that

$$\Gamma_\beta(2)=\Gamma_\beta(0)=\gamma_\beta \quad \text{and} \quad \gamma_{ba}\ll\gamma_\beta. \quad (53)$$

This particular case of a zero coupling will be studied later. The existence of a coupling can be interpreted with the help of the diagram of the transition (Fig. 2).

When condition (53) is fulfilled, the set of transitions represented by the dashed lines of Fig. 2 is not coupled to the set of continuous lines. The b transverse alignment, which corresponds to the Zeeman coherence between the $m_b=-1$ and $m_b=+1$ sublevels, is only coupled to the population of the $m_a=0$ sublevel, whatever the number of absorptions or stimulated emissions of laser photons may be. Then the alignments of b and a are not coupled, for any laser intensity.

When depolarizing relaxation processes exist [$\Gamma_\beta(2)>\Gamma_\beta(0)$], a coupling is induced in three steps: (a) *An interaction with a laser photon* couples the coherence between the $m_b=-1$ and $m_b=+1$ sublevels to the populations of these sublevels. (b) These populations are transferred into the $m_b=0$

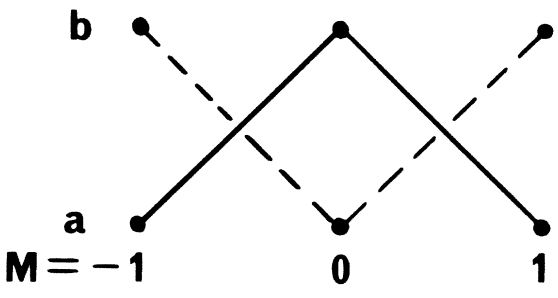

FIG. 2. Diagram of a $J=1$-$J=1$ transition.

sublevel by a *relaxation-induced transition*. (c) *A second interaction with the laser* couples the $m_b = 0$ sublevel to the Zeeman coherence of level a. This coupling involves two interactions with the laser; this is the reason why the first term in the perturbation development of $\gamma\chi_{ba}$ is proportional to γ^2. In order to study the quantitative importance of this coupling, we introduce the normalized alignments $L_2^2(H)$ [Eq. (27)] in (51). Using relations (43), we obtain

$$\frac{[\gamma_a^I(2)]^2+4\omega_a^2}{\Gamma_a(2)+\frac{1}{6}\gamma}\,\frac{{}_aL_2^2(H)}{\Gamma_a^*(2)}-\left[\frac{\gamma}{6}\chi_{ba}+\frac{\gamma_{ba}}{2}\left(1-\frac{4\omega_a\omega_b}{[\Gamma_a(2)+\frac{1}{6}\gamma][\Gamma_b(2)+\frac{1}{6}\gamma]}\right)\right]\frac{{}_bL_2^2(H)}{\Gamma_b(2)}=\frac{M_0^{11}}{\Delta}\left[1+\gamma\left(\frac{\tau_2^2}{4}-\frac{\tau_2^1}{12}\right)\right], \tag{54a}$$

$$-\frac{\gamma}{6}\chi_{ab}\,\frac{{}_aL_2^2(H)}{\Gamma_a^*(2)}+\frac{[\gamma_b^I(2)]^2+4\omega_b^2}{\Gamma_b(2)+\frac{1}{6}\gamma}\,\frac{{}_bL_2^2(H)}{\Gamma_b(2)}=\frac{M_0^{11}}{\Delta}\left[1+\gamma\left(\frac{\tau_2^2}{4}+\frac{\tau_2^1}{12}\right)\right], \tag{54b}$$

where

$$\gamma_\beta^I(2)=\{[\Gamma_\beta(2)+\tfrac{1}{6}\gamma][\Gamma_\beta(2)+\tfrac{1}{6}\gamma\chi_{\beta\beta}]\}^{1/2}. \tag{55}$$

It is possible to verify that, in zero magnetic field, the solution of (54) is ${}_aL_2^2={}_bL_2^2=1$

1. *Coupling by spontaneous emission*

This coupling is of the order of $\gamma_{ba}/2\Gamma_b(2)$ in zero field and, in strong field, of the order of

$$-\frac{\gamma_{ba}}{2\Gamma_b(2)}\,\frac{g_a}{g_b}\,\frac{\Gamma_b(2)+\frac{1}{6}\gamma\chi_{bb}}{\Gamma_a(2)+\frac{1}{6}\gamma}. \tag{56}$$

To find (56), we have assumed that ${}_bL_2^2(\infty)\simeq[\gamma_b^I(2)/2\omega_b]^2$ [see later Eq. (59)]. In the experimental conditions of the 6401-Å neon line [see caption of Fig. 3: $\gamma_{ba}=0.2$ MHz and $\Gamma_b(2)=6.6$ MHz], the coupling in zero field or in strong field are nearly equal to 1.5%, independently of the laser intensity.

2. *Laser-induced coupling*

Neglecting the transfer by spontaneous emission [$\gamma_{ba}=0$ in (54a)] and introducing the following coupling coefficients,

$$\epsilon_{ab}=\frac{\gamma}{6\Gamma_a^*(2)}\,\frac{\chi_{ab}\Delta}{M_0^{11}[1+\gamma(\frac{1}{4}\tau_2^2+\frac{1}{12}\tau_2^1)]}, \tag{57a}$$

$$\epsilon_{ba}=\frac{\gamma}{6\Gamma_b(2)}\,\frac{\chi_{ba}\Delta}{M_0^{11}[1+\gamma(\frac{1}{4}\tau_2^2-\frac{1}{12}\tau_2^1)]}, \tag{57b}$$

we may reduce (54) to the compact shape (β, $\alpha=a$ or b)

$$\left[1+\left(\frac{2\omega_\beta}{\gamma_\beta^I(2)}\right)^2\right]{}_\beta L_2^2(H)=\frac{1+\epsilon_{\alpha\beta}\,{}_\alpha L_2^2(H)}{1+\epsilon_{\alpha\beta}}. \tag{58}$$

Figure 3 shows the numerical importance of the coupling coefficients for the 6401-Å neon line. For high laser intensities, the asymptotic values of ϵ_{ab} and ϵ_{ba} are equal to 2.3% and 4.2%, respectively.

Since the coupling is weak, we can neglect it, in a first approximation. Then the Hanle effects have a Lorentzian shape of half-width $\gamma_\beta^I(2)$;

$${}^{(0)}_\beta L_2^2(H)=\left[1+\left(\frac{2\omega_\beta}{\gamma_\beta^I(2)}\right)^2\right]^{-1}. \tag{59}$$

$\gamma_\beta^I(2)$ is the effective relaxation rate of the transverse alignment. If, in a second approximation, we reintroduce the coupling, then the Hanle effects no longer keep a Lorentzian shape

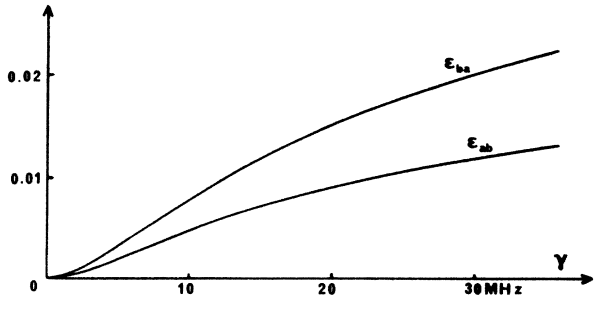

FIG. 3. Laser-induced couplings between the alignments of a $J_b=1$-$J_a=1$ transition. The relaxation rates are, in MHz, $\Gamma_a(0)=8.4$, $\Gamma_a(2)=10.1$, $\Gamma_b(0)=4.4$, $\Gamma_b(2)=6.6$, and $\gamma_{ba}=0.2$. This approximately corresponds to 1 torr of a 10%-90% neon-helium mixture, for the $3s_2$-$2p_2$ neon transition ($\lambda=6401$ Å).

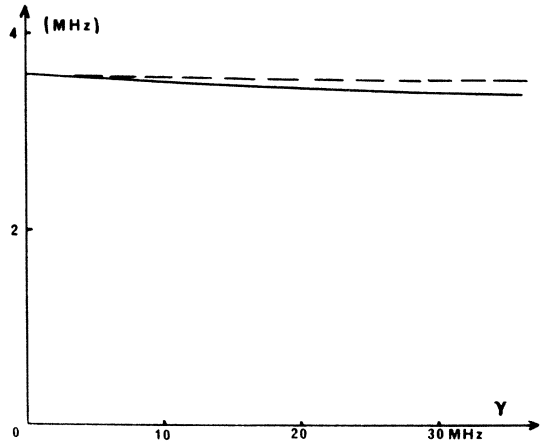

FIG. 4. Difference between the Hanle-effects widths for a $J_b=1$-$J_a=1$ transition. Continuous curve: $\Gamma_a^I(2)-\Gamma_b^I(2)$. Dashed curve: $\gamma_a^I(2)-\gamma_b^I(2)$ (experimental conditions of Fig. 3 with, in addition, $g_a=g_b$).

$$ {}_{\beta}L_2^2(H) = {}^{(0)}_{\beta}L_2^2(H)\,\frac{1+\epsilon_{\alpha\beta}\,{}^{(0)}_{\alpha}L_2^2(H)}{1+\epsilon_{\alpha\beta}}. \tag{60} $$

Now, the half-height half-width is given by

$$ \Gamma_\beta^I(2) = \gamma_\beta^I(2)\left(1-\frac{\epsilon_{\alpha\beta}[g_\alpha\gamma_\beta^I(2)]^2}{[g_\alpha\gamma_\beta^I(2)]^2+[g_\beta\gamma_\alpha^I(2)]^2}\right). \tag{61} $$

In general, the widths of the a and b Hanle effects are not very different. In fact, since the couplings are weak, the deviations from a Lorentzian shape cannot be observed; this has been verified in experiments using the 6401-Å laser line of neon.[14]

3. *Power-broadening of the Hanle effects*

The fourth-order power broadening is obtained from a perturbation development of (55);

$$ \gamma_\beta^I(2) - \Gamma_\beta(2) \simeq \tfrac{1}{6}\gamma. \tag{62} $$

This broadening, which is proportional to the pumping rate, is the same for the two levels. As a matter of fact, this equality between the power-broadenings is nearly maintained in the exact theory [Eqs. (55) and (61)]. Figure 4 shows the difference between the Hanle-effects widths for the 6401-Å line; $\gamma_a^I(2)-\gamma_b^I(2)$ and $\Gamma_a^I(2)-\Gamma_b^I(2)$ are practically independent of the laser intensity. Experimental equality of the power broadenings has been already observed.[14] Experimental tests of Eq. (61) and subsequent measurements of γ have been performed and will be presented in a forthcoming publication.[15]

C. Saturation resonances

The longitudinal components are obtained by means of Eqs. (18);

$$ \Gamma_b(0)\,{}_b\rho_0^0 = -\Gamma_a^*(0)\,{}_a\rho_0^0 = \tfrac{2}{3}\gamma X^1, \tag{63a} $$

$$ \Gamma_b(2)\,{}_b\rho_0^2 = -\frac{\gamma}{3\sqrt{2}}(X^1 - 3X^2), \tag{63b} $$

$$ \Gamma_a(2)\,{}_a\rho_0^2 = \frac{\gamma X^1}{3\sqrt{2}}\left(1+\frac{\gamma_{ba}}{2\Gamma_b(2)}\right)+\frac{\gamma X^2}{\sqrt{2}}\left(1-\frac{\gamma_{ba}}{2\Gamma_b(2)}\right). \tag{63c} $$

Equations (63), combined with (48), show that the populations of the levels exhibit zero-field resonance, which is the sum of two contributions proportional to the Hanle effect of the a level and of the b level, respectively. For instance, for the b level, we obtain

$$ \Gamma_b(0)\,{}_b\rho_0^0 = -\frac{2n\gamma}{3\Delta\sqrt{3}}\left(1+\frac{\tau_2^2}{4}\gamma-\gamma\,\frac{1+(\frac{1}{4}\tau_2^2+\frac{1}{12}\tau_1^2)\gamma}{12M_0^{11}}\,\frac{{}_bL_2^2(H)}{\Gamma_b(2)}-\gamma\,\frac{1+(\frac{1}{4}\tau_2^2-\frac{1}{12}\tau_1^2)\gamma}{12M_0^{11}}\,\frac{{}_aL_2^2(H)}{\Gamma_a^*(2)}\right), \tag{64a} $$

$$ \Gamma_b(2)\,{}_b\rho_0^2 = \frac{n\gamma}{3\Delta\sqrt{6}}\left(1+\frac{\gamma}{2\Gamma_a(2)}+\gamma\,\frac{1+[\frac{1}{3}\tau(0)-1/6\Gamma_a(2)]\gamma}{6M_0^{11}}\,\frac{{}_bL_2^2(H)}{\Gamma_b(2)}-\gamma\,\frac{1+[\tau(0)+1/\Gamma_a(2)]\frac{1}{6}\gamma}{3M_0^{11}}\,\frac{{}_aL_2^2(H)}{\Gamma_a^*(2)}\right). \tag{64b} $$

This resonance may be observed on the π components of the fluorescent lines emitted by the laser levels. For a fluorescent line $b\to g$, the intensity is proportional to[3]

$$ L_{bg}^{\pi} = {}_b\rho_0^0 + A_g\,{}_b\rho_0^2\sqrt{2}, \tag{65} $$

where $A_g = -1$, $\frac{1}{2}$, or $-\frac{1}{10}$ if $J_g = 0$, 1, or 2, respectively. The relative amplitude of the saturation resonance, $[L^\pi(\infty)-L^\pi(0)]/L^\pi(\infty)$, is given by

$$ S_{bg} = 1-\frac{\Delta}{M_0^{11}}\,\frac{1-A_g\Gamma_b(0)/2\Gamma_b(2)}{1+\gamma\tfrac{1}{4}\tau_2^2-A_g[\Gamma_b(0)/2\Gamma_b(2)][1+\gamma/2\Gamma_a(2)]}. \tag{66} $$

Equations (64)–(66) show that, in general the shape and the amplitude of the saturation resonance depend on the fluorescence line, contrary to the case of a $J=1$-$J=0$ laser line. This is due to the fact that population and longitudinal alignment are not proportional. Experimental verifications of these theoretical results will be published later.[15]

D. Particular cases

There are two particular cases, for which the Hanle effects are exactly Lorentzian.

1. *Equality of the relaxation times of the two alignments*

Equation (48b) shows that, in strong magnetic fields, X^2 is proportional to τ_2^1. The optical quadrupole moment has the same sign as $\Gamma_b(2)-\Gamma_a^*(2)$. When $\Gamma_b(2)$ and $\Gamma_a^*(2)$ are equal (49), this moment vanishes. Then, in strong fields, all the longitudinal components of the density matrix are proportional, independent of the laser intensity.

If, in addition, the Landé factors are equal, it is possible to show that the two Hanle effects are proportional. Indeed, when $\Gamma_a^*(2)=\Gamma_b(2)$ and $\omega_a=\omega_b$, the *exact* solution of (54) is given by

$$ {}_aL_2^2 = {}_bL_2^2 = \{1+[2\omega_b/\Gamma_b^I(2)]^2\}^{-1}, \tag{67} $$

where

$$ \Gamma_b^I(2) = \gamma_b^I(2)(1+\epsilon_{ab})^{-1/2} = \left[[\Gamma_b(2)+\tfrac{1}{6}\gamma]\times\left(\Gamma_b(2)+\frac{\frac{1}{6}\gamma}{1+\frac{2}{9}\gamma[\tau(0)+1/4\Gamma_b(2)]}\right)\right]^{1/2}. \tag{68} $$

The Hanle effects always keep a Lorentzian shape, independently of the coupling of the transverse alignments. Equation (67) involves the facts that ${}_aR_2^2(H) = -{}_bR_2^2(H)$, and subsequently that X^2 vanishes whatever the magnetic field may be. All the longitudinal components are proportional to X^1 and exhibit a Lorentzian saturation resonance of shape ${}_bL_2^2$ and of amplitude

$$\mathcal{S} = -\frac{{}_bR_2^2(0)}{n} = \frac{\gamma}{6\Gamma_b(2)}\left[1+\frac{2\gamma}{9}\left(\tau(0)+\frac{1}{\Gamma_b(2)}\right)\right]^{-1}. \quad (69)$$

In this case, the saturation resonance does not depend on the fluorescence lines.

2. *Two-relaxation-times model*

When conditions (53) are fulfilled (one relaxation time per level, and no coupling by spontaneous emission), the transverse alignments are not coupled. The Hanle effects are Lorentzian, and their widths are given by $\gamma_\beta^I(2)$ [Eq. (55)]. On the other hand, the intensity of the π fluorescent line $b \to g$ is given by [Eqs. (63) and (48)]

$${}_b\rho_0^0 - \sqrt{2}\,{}_b\rho_0^2 = -\frac{\gamma}{\gamma_b\sqrt{3}}\,\frac{n - {}_aR_2^2(H)}{1+\frac{1}{3}\gamma(1/\gamma_b+1/2\gamma_a)}, \quad (70)$$

if $J_g = 0$, and

$${}_b\rho_0^0 + \frac{{}_b\rho_0^2}{\sqrt{2}} = -\frac{\gamma}{2\gamma_b\sqrt{3}}\,\frac{n + {}_bR_2^2(H)}{1+\frac{1}{3}\gamma(1/\gamma_a+1/2\gamma_b)}, \quad (71)$$

if $J_g = 1$.

These results can be interpreted with the diagram of Fig. 2. If there is no relaxation-induced transfer between the Zeeman sublevels, the set of dashed lines of Fig. 2 and the set of solid lines are decoupled. For each set, the diagram of the transitions is similar to the one of a $J=1$-$J=0$ line; in the same way as it is for this line, the Hanle effects have a Lorentzian shape. Indeed it is easy to show that, when (53) is fulfilled, Eq. (55) for $\gamma_b^I(2)$ is exactly equivalent to Eq. (36), where $\frac{1}{3}\gamma$ is replaced by $\frac{1}{6}\gamma$. On the other hand, the intensity of the π-polarized fluorescent line $b \to g$ is proportional to the population of the $m_b = 0$ sublevel, if $J_g = 0$, and to the populations of the $m_b = \pm 1$ sublevels, if $J_g = 1$. Subsequently the $J_b = 1$-$J_g = 0$ fluorescence is connected to the Hanle effect of a only (by the solid lines), and the $J_b = 1$-$J_g = 1$ fluorescence is connected to the b Hanle effect only (set of dashed lines). This explains why the saturation resonance is proportional to ${}_aR_2^2$ in (70) and to ${}_bR_2^2$ in (71). For the fluorescence emitted by the a level, the arguments are reversed.

V. TRANSITION $J_b = 1 \to J_a = 2$

Up to now, for $J=1$-$J=0$ and $J=1$-$J=1$ transitions, the laser irradiation induced population and alignment only in the excited levels. These quantities appeared in the second-order terms ("linear response"). On the other hand, if the transition is a $J_b = 1 \to J_a = 2$ one, the laser may induce ${}_a\rho_Q^4$ components in the atomic density matrix. These are the components of an electric hexadecapole moment, which is created in the a level from the fourth order in the laser field. There are four quantities which precess in the magnetic field: alignments of levels a (${}_a\rho_2^2$) and b (${}_b\rho_2^2$), and hexadecapole moment of a (${}_a\rho_2^4$, ${}_a\rho_4^4$). The equations of motion are very complicated, and we shall be obliged to introduce a great number of notations. In order to simplify the presentation of the theory, these notations have been put together in Appendix A.[16]

A. Zero magnetic field: Anisotropy ratio of the fluorescent lines

In Appendix A, we define the times $\tau(0)$, $\tau(4)$, and τ_j^i [(A1)-(A4)]. Matrix M_0 may be expressed as a function of these quantities (A5). The inversion of this matrix is easily performed and leads to the following values of the density-matrix components [for a π polarization of the laser; Eqs. (6)-(10)]:

$$\Gamma_a^*(0)\,{}_a\sigma_0^0 = -\sqrt{\tfrac{3}{5}}\,\Gamma_b(0)\,{}_b\sigma_0^0 = \frac{2n\gamma}{3\Delta_0\sqrt{5}}\left[1+\left(\frac{8\tau(4)}{35}+\frac{6\tau_3^3}{25}\right)\gamma\right], \quad (72a)$$

$$\Gamma_b(2)\,{}_b\sigma_0^2 = \frac{n\gamma\sqrt{2}}{15\Delta_0\sqrt{3}}\left[1+\frac{8\gamma}{35}\left(\frac{1}{\Gamma_a(4)}-\frac{1}{\Gamma_a(2)}\right)\right], \quad (72b)$$

$$\Gamma_a^*(2)\,{}_a\sigma_0^2 = -\frac{n\gamma\sqrt{14}}{15\Delta_0}\left[1+\frac{8\gamma}{35}\left(\frac{1}{\Gamma_a(4)}+\frac{1}{\Gamma_b(2)-\frac{1}{10}\gamma_{ba}}\right)\right], \quad (72c)$$

$$\Gamma_a(4)\,{}_a\sigma_0^4 = -\frac{4n\gamma\sqrt{2}}{75\Delta_0\sqrt{35}}\,\gamma\tau_3^1, \quad (72d)$$

where Δ_0 is the determinant of M_0 [polynomial quadratic in γ, see Eq. (A6)]. $\Gamma_a^*(0)$ is given by (30) and $\Gamma_a^*(2)$ by

$$\Gamma_a^*(2) = \Gamma_a(2)[1-\gamma_{ba}/10\Gamma_b(2)]^{-1}. \quad (73)$$

The density matrix for a σ-polarized laser in a zero magnetic field is obtained from (11);

$$\rho_2^2(0)\sqrt{\tfrac{2}{3}} = -\rho_0^2(0) = \tfrac{1}{2}\sigma_0^2, \quad (74a)$$

$$\rho_4^4(0)\sqrt{\tfrac{2}{35}} = -\rho_2^4(0)/\sqrt{10} = \tfrac{1}{3}\rho_0^4(0) = \tfrac{1}{8}\sigma_0^4. \quad (74b)$$

These components may be analysed with the help of the zero-field anisotropy of the laser-induced change of the fluorescent lines. This anisotropy is defined by the zero-field ratio between the

anisotropic part of the fluorescent line, which is connected to the transverse alignment, and the isotropic part, connected to the population and to the longitudinal alignment. (For a precise definition of the anisotropy ratio, and the way of measuring it, see Refs. 3 and 8–10.) Using (74a), we obtain for the anisotropy of the $\beta \rightarrow \alpha$ fluorescence [Eq. (5) of Ref. 10]

$$R_{\beta\alpha} = (-)^{J_\beta + J_\alpha + 1} 3 \begin{Bmatrix} 1 & 1 & 2 \\ J_\beta & J_\beta & J_\alpha \end{Bmatrix} \Bigg/ \left[\left(\frac{2}{3(2J_\beta+1)} \right)^{1/2} \frac{{}_\beta\rho_0^0(0)}{{}_\beta\rho_0^2(0)} + (-)^{J_\beta + J_\alpha + 1} \begin{Bmatrix} 1 & 1 & 2 \\ J_\beta & J_\beta & J_\alpha \end{Bmatrix} \right] \quad (\beta = a \text{ or } b). \tag{75}$$

For $J = 1 \rightarrow J = 0$ and $J = 1 \rightarrow J = 1$ transitions, ρ_0^0 and ρ_0^2 are proportional, and the anisotropy does not depend on the power of irradiation. For a $J = 1 \rightarrow J = 2$ transition, owing to the fact that, in addition to the electric dipole moment, an optical octopole moment (${}_{ab}\rho_{Q'}^3$) is created at high laser intensities, ρ_0^2 and ρ_0^0 are not proportional. For each laser level, ρ_0^2/ρ_0^0 exhibits homographic variations with γ. Subsequently R depends on the laser intensity; the degree of polarization of the fluorescence decreases with increasing laser intensities.

For the a level. This depolarization of the fluorescence is very weak because the ratio ${}_a\rho_0^2/{}_a\rho_0^0$ is not very dependent on γ. Indeed, if $\Gamma_a(4) = \Gamma_a(2)$, then ${}_a\rho_0^2/{}_a\rho_0^0$ is reduced 4% when γ grows from zero to infinity. Figure 5 shows the variations of the anisotropy for $J_a \rightarrow J_f = 2$ and $J_a \rightarrow J_f = 1$ fluorescent lines (experimental conditions of note[16]). The anisotropy is practically independent of the laser intensity, as it has been observed experimentally (Fig. 6 of Ref. 8).

For the b level. The variations of ρ_0^2/ρ_0^0 with γ are shown in Fig. 6. Since ${}_b\rho_0^2/{}_b\rho_0^0$ is very small, the anisotropy ratio R_{bg} is fairly well proportional to ${}_b\rho_0^2/{}_b\rho_0^0$, independently of the fluorescent line ($J_g = 0$, 1, or 2). Depolarization of the fluorescence, similar to the one predicted by Fig. 6, has been observed experimentally[9,17] (for instance, see Fig. 4 of Ref. 9). At strong laser intensities, ${}_b\rho_0^2/{}_b\rho_0^0$ becomes proportional to $\Gamma_a(2)$-$\Gamma_a(4)$ [see (72b)]. In particular, in the case when $\Gamma_a(4) > \Gamma_a(2)$, the anisotropy is reversed, at high intensities. Since the anisotropy is very sensitive to the difference between the quadrupole and hexadecapole relaxation rates of the a level, the study of the variations of R_{bg} with the laser intensity must allow the measurement of $\Gamma_a(4)$ [$\Gamma_a(2)$ may be obtained from the width of the a Hanle effect]. Experiments on this point, using the 6328-Å neon line, are in progress.[18]

B. Hanle effects: Laser-induced hexadecapole moment in the a level

When the magnetic field is different from zero, we must use Eqs. (25) and (26). Quantities $X^{k'}$ verify the matrix equation (21):

$$M \begin{pmatrix} X^1 \\ X^2 \\ X^3 \end{pmatrix} = \begin{pmatrix} -\frac{n}{\sqrt{3}} + \frac{{}_bR_2^2}{10\sqrt{3}} - \frac{\sqrt{7}}{10}\,{}_aR_2^2 \\ \frac{{}_bR_2^2}{2\sqrt{15}} - \frac{\sqrt{7}}{6\sqrt{5}}\,{}_aR_2^2 \\ \frac{{}_bR_2^2}{5\sqrt{3}} - \frac{{}_aR_2^2}{15\sqrt{7}} - \frac{\sqrt{3}}{2\sqrt{7}}\,{}_aR_4^2 \end{pmatrix}, \tag{76}$$

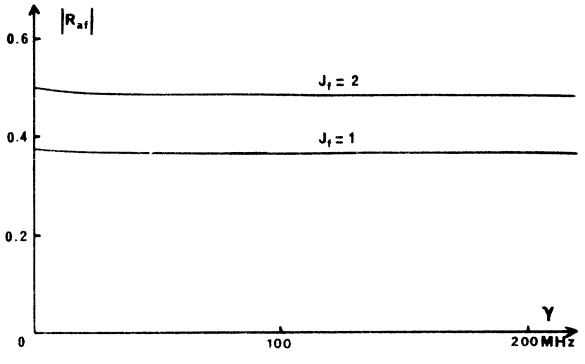

FIG. 5. Zero-field anisotropy ratios of the Fluorescent lines from the a level, as functions of the pumping rate [$J_b = 1 \rightarrow J_a = 2$ laser transition; experimental conditions of note (Ref. 16)].

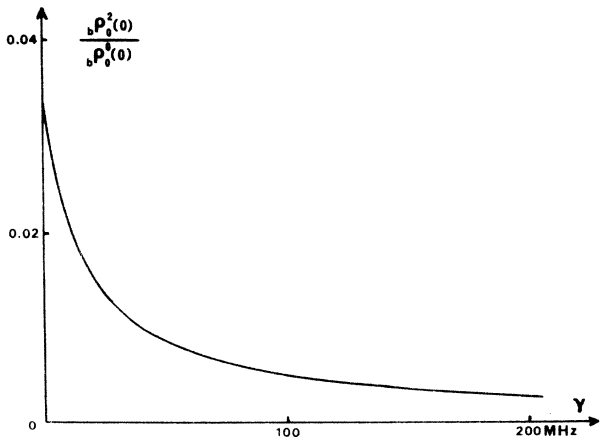

FIG. 6. Alignment to population ratio for the b level in zero magnetic field [$J_b = 1 \rightarrow J_a = 2$ transition; experimental conditions of note (Ref. 16)].

where matrix M is given by Eq. (A7). Then, $X^{k'}$ is obtained with the help of the inverse matrix μ/Δ [(A8), (A9)] and, when replaced in (25), leads to the following equations of motion for the transverse components of the density matrix:

$$\left(\Gamma_a(2)+\frac{5\gamma}{42}+2i\omega_a\right){}_a\rho_2^2-\left(\frac{2\gamma}{5\sqrt{21}}+\frac{\sqrt{21}}{10}\gamma_{ba}\right){}_b\rho_2^2+\frac{\gamma}{35\sqrt{3}}\,{}_a\rho_2^4-\frac{\gamma}{5\sqrt{21}}\,{}_a\rho_4^4$$
$$=-\frac{n\gamma\sqrt{7}}{10\sqrt{3}}\,\chi_a^2+\frac{23\gamma}{210}\left(1-\chi_{aa}^{22}\right){}_aR_2^2-\frac{\gamma}{5\sqrt{21}}\left(1-\chi_{ba}^{22}\right){}_bR_2^2+\frac{\gamma}{70\sqrt{3}}\left(1-\chi_{aa}^{42}\right){}_aR_2^4, \quad (77a)$$

$$-\frac{2\gamma}{5\sqrt{21}}\,{}_a\rho_2^2+\left(\Gamma_b(2)+\frac{7\gamma}{30}+2i\omega_b\right){}_b\rho_2^2-\frac{\gamma}{5\sqrt{7}}\,{}_a\rho_2^4+\frac{\gamma}{5}\,{}_a\rho_4^4$$
$$=\frac{n\gamma}{30}\,\chi_b^2-\frac{\gamma}{5\sqrt{21}}\left(1-\chi_{ab}^{22}\right){}_aR_2^2+\frac{\gamma}{30}\left(1-\chi_{bb}^{22}\right){}_bR_2^2-\frac{\gamma}{10\sqrt{7}}\left(1-\chi_{ab}^{42}\right){}_aR_2^4, \quad (77b)$$

$$\frac{\gamma}{35\sqrt{3}}\,{}_a\rho_2^2-\frac{\gamma}{5\sqrt{7}}\,{}_b\rho_2^2+\left(\Gamma_a(4)+\frac{4\gamma}{35}+2i\omega_a\right){}_a\rho_2^4-\frac{\gamma}{10\sqrt{7}}\,{}_a\rho_4^4$$
$$=\frac{n\gamma}{15\sqrt{7}}\,\chi_a^4+\frac{\gamma}{70\sqrt{3}}\left(1-\chi_{aa}^{24}\right){}_aR_2^2-\frac{\gamma}{10\sqrt{7}}\left(1-\chi_{ba}^{24}\right){}_bR_2^2+\frac{3\gamma}{28}\left(1-\chi_{aa}^{44}\right){}_aR_2^4, \quad (77c)$$

$$-\frac{\gamma}{5\sqrt{21}}\,{}_a\rho_2^2+\frac{\gamma}{5}\,{}_b\rho_2^2-\frac{\gamma}{10\sqrt{7}}\,{}_a\rho_2^4+\left(\Gamma_a(4)+\frac{\gamma}{5}+4i\omega_a\right){}_a\rho_4^4=0, \quad (77d)$$

where the coefficients χ are given by (A10) and (A11).

In the left-hand side of these equations, we have put together the effects of the relaxation processes, of the magnetic field, of the spontaneous transfer of alignment from b to a, and of the direct laser-induced coupling between the transverse components. The right-hand side contains the excitation term (with n) and the indirect coupling through the sublevels populations (R terms). We shall note that (77a)–(77d) correspond to the equations of motion of ${}_a\rho_2^2$, ${}_b\rho_2^2$, ${}_a\rho_2^4$, and ${}_a\rho_4^4$, respectively; indeed, at weak laser intensities, when the laser-induced couplings are small, each of the equations determine the corresponding density-matrix component.

In general, it is not possible to find the analytic solution of Eqs. (77).[19] First we shall calculate an approximate solution which gives a straightforward physical interpretation of the observed effects. Second, an exact computer calculation will be presented, and its results will be compared with the approximate solution.

1. *Approximate solution*

a. Hanle effect of a. An important point is that the alignment of b is much smaller than the alignment of a (this is the well-known fact that the optical pumping of a $J=1$ level using a $J=1$-$J=2$ transition is not very efficient).[8,9] This may be verified in zero magnetic field by means of Eqs. (72). On the other hand, the hexadecapole moment (${}_a\rho_2^4$, ${}_a\rho_4^4$) is also small compared to the alignment of a. Subsequently, in Eq. (77a), the laser-induced couplings of ${}_b\rho_2^2$, ${}_a\rho_2^4$, and ${}_a\rho_4^4$ with ${}_a\rho_2^2$ are weak. For instance, we can define the importance of the zero-field coupling ${}_b\rho_2^2 \rightarrow {}_a\rho_2^2$ by the ratio

$$\frac{2\gamma/5\sqrt{21}+\sqrt{21}\gamma_{ba}/10}{\Gamma_a(2)+\frac{5}{42}\gamma}\,\frac{{}_b\rho_2^2(0)}{{}_a\rho_2^2(0)}. \quad (78)$$

This ratio may be evaluated using (72)–(74). With conditions of note,[16] it has a maximum value of 3.3%, when γ is equal to 40 MHz. The ${}_a\rho_4^4$ and ${}_a\rho_2^4$ couplings are maxima when γ is infinite, and are respectively equal to 2% and 7%. In the same way, we can neglect the couplings with ${}_bR_2^2$ and ${}_aR_2^4$, which are of the same order of magnitude, and (77a) is reduced to

$$\left(\Gamma_a(2)+\frac{5\gamma}{42}+2i\omega_a\right){}^{(0)}_a\rho_2^2$$
$$=-\frac{n\gamma\sqrt{7}}{10\sqrt{3}}\,\chi_a^2+\frac{23\gamma}{210}\left(1-\chi_{aa}^{22}\right){}^{(0)}_aR_2^2. \quad (79)$$

This equation and its complex conjugate lead to a Lorentzian shape for the a Hanle effect;

$${}^{(0)}_aR_2^2(H)=-\frac{n\gamma\sqrt{7}}{10\sqrt{3}}\,\frac{\left[\Gamma_a(2)+\frac{5}{42}\gamma\right]\chi_a^2}{\left[\gamma_a^I(2)\right]^2+4\omega_a^2}, \quad (80a)$$

$${}^{(0)}_a\rho_2^2(H)={}^{(0)}_aR_2^2(H)\left(1-\frac{2i\omega_a}{\Gamma_a(2)+\frac{5}{42}\gamma}\right). \quad (80b)$$

The width is given by

$$\gamma_a^I(2)=\left(\Gamma_a(2)+\frac{5\gamma}{42}\right)\left(1-\frac{23\gamma}{210}\,\frac{1-\chi_{aa}^{22}}{\Gamma_a(2)+\frac{5}{42}\gamma}\right)^{1/2}. \quad (81)$$

The variations of $\gamma_a^I(2)$ with γ are shown in Fig. 7 (continuous curve) for the experimental situation

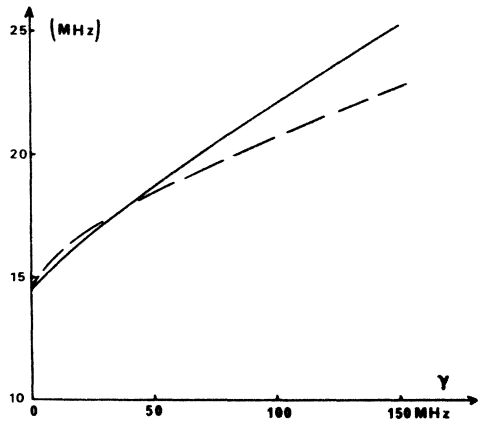

FIG. 7. Power broadening of the a Hanle effect ($J_b=1$-$J_a=2$ transition; experimental conditions of note (Ref. 16)]. Continuous curve: approximate solution $\gamma_a^I(2)$ (coupling-free Hanle effect). Dashed curve: exact computer calculation.

of note.[16] However, we must point out that Eqs. (80) fail at strong laser intensities. Indeed the zero-field value of (80) is

$$ {}^{(0)}_{a}\rho_2^2(0) = -\frac{n\gamma\sqrt{7}}{10\sqrt{3}} \frac{\chi_a^2}{\Gamma_a(2)+\frac{5}{42}\gamma-\frac{23}{210}\gamma(1-\chi_{aa}^{22})}, \tag{82} $$

while the exact value is [Eqs. (72)–(74)]

$$ {}_{a}\rho_2^2(0) = -\frac{n\gamma\sqrt{7}}{10\Gamma_a^*(2)\Delta_0\sqrt{3}}\left[1+\frac{8\gamma}{35}\left(\frac{1}{\Gamma_a(4)}+\frac{1}{\Gamma_b(2)-\frac{1}{10}\gamma_{ba}}\right)\right]. \tag{83} $$

As a matter of fact, ${}^{(0)}_{a}\rho_2^2(0)$ goes to zero at strong laser intensities, while the exact solution does not vanish. This is due to the fact that χ_a^2 vanishes when γ is infinite. Subsequently, at very high intensities, the couplings with ${}_{b}\rho_2^2$, ${}_{a}\rho_4^4$, and ${}_{a}\rho_2^4$ are not negligible compared to the source term $n\chi_a^2$ (though these couplings are weak compared to ${}_{a}\rho_2^2$). In order to study the magnitude of the neglected terms, we can consider $[{}_{a}\rho_2^2(0)-{}^{(0)}_{a}\rho_2^2(0)]/{}_{a}\rho_2^2(0)$. In the conditions of Ref. 16, this quantity is equal to 3% and 8%, when γ is equal to 100 and 200 MHz, respectively. For these values of γ, the approximations are fairly valid. Assuming that the Hanle-effect shape given by (80a) is correct, we can "renormalize" its amplitude with

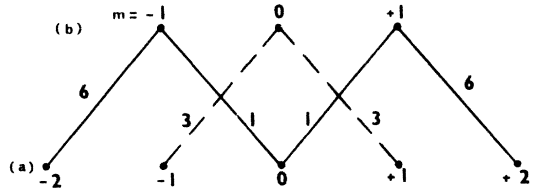

FIG. 8. Diagram of a $J=1$-$J=2$ transition, with the relative transition probabilities.

the exact zero-field solution. (80a) is then replaced by

$$ {}^{(0)}_{a}R_2^2(H) = {}_{a}\rho_2^2(0)\,{}^{(0)}_{a}L_2^2(H), \tag{84} $$

where ${}_{a}\rho_2^2(0)$ is the exact zero-field solution (83) and where

$$ {}^{(0)}_{a}L_2^2(H) = \{1+[2\omega_a/\gamma_a^I(2)]^2\}^{-1}. \tag{85} $$

b. Laser-induced hexadecapole moment in level a. Equation (77d) shows that a $\Delta m=4$ Zeeman coherence (${}_{a}\rho_4^4$) is created by the laser in the a level. This process can be understood with the help of the diagram of the transition (Fig. 8). For instance, the stimulated emission of a linearly σ-polarized photon creates coherence between the $m_a=\pm 2$ sublevels from the Zeeman coherence between the $m_b=\pm 1$ sublevels (through the transitions represented by solid lines in Fig. 8). This corresponds to the creation of ${}_{a}\rho_4^4$ from ${}_{b}\rho_2^2$. In the same way, from the $\Delta m=2$ coherence in level a (${}_{a}\rho_2^2$ and ${}_{a}\rho_2^4$), the absorption of a laser photon induces $\Delta m=4$ coherence (for instance, by adding coherence $m_a=0 \leftrightarrow m_a=-2$ to coherence $m_a=0 \leftrightarrow m_a=2$).

To solve (77d), we shall neglect the ${}_{a}\rho_2^4$ and ${}_{b}\rho_2^2$ terms. Indeed, on the one hand, the ${}_{a}\rho_2^4$ contribution is never more than 10% of the ${}_{a}\rho_2^2$ contribution. On the other hand, ${}_{a}\rho_4^4$ is *important at high intensities only*, because it appears from the fourth order in the laser field. Since ${}_{b}\rho_2^2(0)$ goes to zero for strong intensities [see Eq. (72b) and Fig. 6], we neglect it compared with ${}_{a}\rho_2^2$. Then (72d) is reduced to

$$ \left(\Gamma_a(4)+\frac{\gamma}{5}+4i\omega_a\right){}^{(0)}_{a}\rho_4^4(H) = \frac{\gamma}{5\sqrt{21}}\,{}_{a}\rho_2^2(H). \tag{86} $$

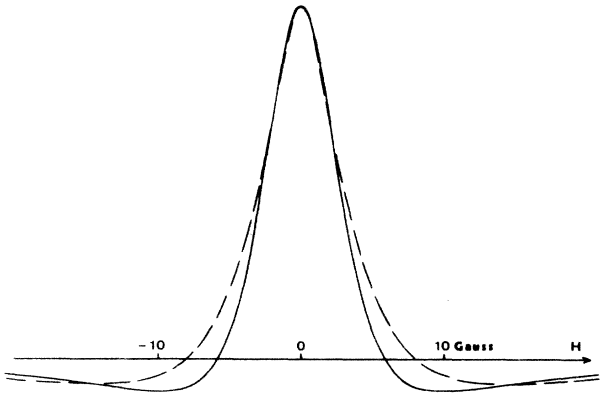

FIG. 9. Variations with the magnetic field of the real part of the hexadecapole moment induced by the laser in the a level ($J_b=1$-$J_a=2$ transition; experimental conditions of note (Ref. 16); pumping rate $\gamma=100$ MHz]. Continuous curve: approximate solution. Dashed curve: exact computer solution.

Obviously, since the approximations leading to (86) are rather crude, (86) is no longer verified by the zero-field solution (72). However, as it has been done for ${}_a\rho_2^2$, (86) may be "renormalized" by replacing $\gamma/5\sqrt{21}$ by $[\Gamma_a(4)+\frac{1}{5}\gamma]_a\rho_4^4(0)/{}_a\rho_2^2(0)$, where ${}_a\rho_4^4(0)$ and ${}_a\rho_2^2(0)$ are the exact zero-field solutions. Using (80b) and (84), we finally obtain

$$ {}^{(0)}_a\rho_4^4(H) = {}_a\rho_4^4(0)\frac{1-2i\omega_a/[\Gamma_a(2)+\frac{5}{42}\gamma]}{1+4i\omega_a/[\Gamma_a(4)+\frac{1}{5}\gamma]}\,{}^{(0)}_aL_2^2(H)\,. \tag{87}$$

The variations of ${}^{(0)}_aR_4^4(H)$ with the magnetic field have been represented in Fig. 9 (solid curve) when the pumping rate γ is equal to 100 MHz. In the same figure, the dashed curve gives the exact solution as obtained by a computer calculation (see Sec. V B 2).

c. Hanle effect of b. In order to obtain the shape of the b Hanle effect, we must solve the equations of motion of the b transverse alignment, (77b). The principal difficulty comes from the fact that this alignment is very small at high laser intensities [see Eq. (72b) and Fig. 6]. Consequently, in (77b), we cannot neglect the various couplings with the ${}_a\rho_2^2$, ${}_a\rho_2^4$, and ${}_a\rho_4^4$ components; their contributions are as large as the direct excitation. Since ${}_a\rho_4^4$ and ${}_a\rho_2^2$ have been previously calculated, the only component to determine is ${}_a\rho_2^4$.

When $\Gamma_a(4)$ is equal to $\Gamma_a(2)$, ${}_a\rho_2^4(H)$ and ${}_a\rho_2^2(H)$, both corresponding to a $\Delta m=2$ Zeeman coherence in the a level, exhibit similar variations with the magnetic field for weak laser intensities. We shall assume that *${}_a\rho_2^4(H)$ and ${}_a\rho_2^2(H)$ are proportional, whatever the intensity may be.* On the other hand, χ_{ab}^{22} and χ_{ab}^{42} have close values [we shall see later that they are exactly equal when there is no depolarizing processes; $\Gamma_\beta(k)=\gamma_\beta$]. Then assuming $\chi_{ab}^{22}=\chi_{ab}^{42}$ and introducing the following parameter,

$$\epsilon = \tfrac{1}{2}\sqrt{3}\,{}_a\rho_2^4(0)/{}_a\rho_2^2(0)\,, \tag{88}$$

Eq. (77b) becomes[20]

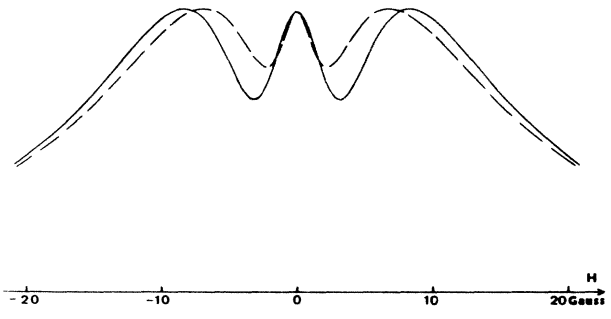

FIG. 10. Hanle effect of level b, in the same conditions as those of Fig. 9. Continuous curve: approximate solution. Dashed curve: exact solution.

$$\left(\Gamma_b(2)+\frac{7\gamma}{30}+2i\omega_b\right){}_b\rho_2^2-\frac{2\gamma}{5\sqrt{21}}(1+\epsilon)\,{}_a\rho_2^2+\frac{\gamma}{5}\,{}_a\rho_4^4$$
$$=\frac{n\gamma}{30}\chi_b^2+\frac{\gamma}{30}(1-\chi_{bb}^{22})\,{}_bR_2^2-\frac{\gamma}{5\sqrt{21}}(1-\chi_{ab}^{22})(1+\epsilon)\,{}_aR_2^2\,. \tag{89}$$

Using Eq. (80b) and eliminating the imaginary part of ${}_b\rho_2^2$ between (89) and its complex conjugate, we obtain

$$\frac{[\gamma_b^I(2)]^2+4\omega_b^2}{\Gamma_b(2)+\frac{7}{30}\gamma}\,{}_bR_2^2(H)$$
$$=\frac{n\gamma}{30}\chi_b^2-\frac{\gamma}{5}\,\mathrm{Re}\left[\left(1-\frac{2i\omega_b}{\Gamma_b(2)+\frac{7}{30}\gamma}\right){}_a\rho_4^4(H)\right]+\frac{\gamma(1+\epsilon)}{5\sqrt{21}}$$
$$\times\left(1+\chi_{ab}^{22}-\frac{8\omega_a\omega_b}{[\Gamma_a(2)+\frac{5}{42}\gamma][\Gamma_b(2)+\frac{7}{30}\gamma]}\right){}_aR_2^2(H)\,, \tag{90}$$

where

$$\gamma_b^I(2)=\left(\Gamma_b(2)+\frac{7\gamma}{30}\right)\left(1-\frac{\gamma}{30}\frac{1-\chi_{bb}^{22}}{\Gamma_b(2)+\frac{7}{30}\gamma}\right)^{1/2}. \tag{91}$$

When the ${}_a\rho_4^4$ and ${}_a\rho_2^2$ terms are neglected in (90), ${}_bR_2^2$ has a Lorentzian shape of width $\gamma_b^I(2)$. This "uncoupled" Hanle effect is strongly power broadened by the laser; for $\gamma=100$ MHz, the power broadening of b is 3 times that of level a. This is due to the strong probability of the transitions issued from the $m_b=\pm1$ sublevels on the one hand, and on the other hand to the weakness of the coherence restitution through the sublevels populations [${}_bR_2^2$ term in (89)]; here, this is possible through the $m_a=0\rightarrow m_b=\pm1$ transitions only, and the relative transition probability is 1 (see Fig. 8).

The $\Delta m=4$ coherence of a is transferred to the b level through the $m_a=\pm2\rightarrow m_b=\pm1$ transitions. This transfer involves the second term of the right-hand side of (90). Since ${}_a\rho_4^4(0)$ is negative, this contribution has the same sign as the direct excitation. The resonance induced by this coupling is very narrow, because ${}_a\rho_4^4$ evolves at 4 times the Larmor frequency.

The $\Delta m=2$ coherence in level a (${}_a\rho_2^2$, ${}_a\rho_2^4$) is transferred to b through either the σ^+ transitions ($m_a=-2\rightarrow m_b=-1$ and $m_a=0\rightarrow m_b=1$), or the σ^- transitions. This coupling has the same sign as ${}_a\rho_2^2(0)$, which is negative [last term of (90)]. The corresponding resonance will appear as a dip in the Hanle effect.

By putting (84), (85), and (87) in (90), we obtain the approximate shape of the Hanle effect. This is shown in Fig. 10 for $\gamma=100$ MHz (continuous curve). On the broad uncoupled Hanle effect, a narrow central resonance appears because of the $\Delta m=4$ coherence of a, and a broader dip because

of the $\Delta m = 2$ coherence of a. The exact solution, obtained by a computer calculation, exhibits the expected shape but the contrast of the resonance is smoothed (dashed curve of Fig. 10).

2. *Computer calculation*

The previous calculation has allowed us to exhibit the principal features of the solution, and to analyze its physical interpretation. But we have obtained results which are essentially qualitative. A quantitative comparison between theory and experiments is possible with the exact solution of (77) only. This solution has been obtained by means of a computer calculation. With the help of the 4×4 matrices Γ, Ω, χ [Eqs. (A13)–(A15)] and of the column vectors ρ, R, and Λ (A16)–(A17), Eqs. (77) may be written as a compact expression

$$(\Gamma + i\Omega)\rho = n\Lambda + \chi R \,. \tag{92}$$

(92) is equivalent to two sets of coupled equations:

$$\Gamma R - \Omega\,\mathrm{Im}(\rho) = n\Lambda + \chi R \,, \quad \Gamma\,\mathrm{Im}(\rho) + \Omega R = 0 \,, \tag{93}$$

where $\mathrm{Im}(\rho)$ is the imaginary part of ρ. Then the formal solution of (93) is

$$R = n(\Gamma - \chi + \Omega\Gamma^{-1}\Omega)^{-1}\Lambda \,. \tag{94}$$

The inversion of matrices Γ and $(\Gamma - \chi + \Omega\Gamma^{-1}\Omega)$ have been performed by a computer for each value of γ and of the magnetic field. Let us analyze the results concerning the Hanle effect.

a. Hanle effect of a. The computer solution shows that the couplings of ${}_a\rho_4^4$, ${}_a\rho_2^4$, and ${}_b\rho_2^2$ with ${}_a\rho_2^2$ are too small for implying any important deviations of the Hanle-effect shape from a Lorentzian one. When $\gamma = 100$ MHz, the deviations are lower than 1% of the total amplitude of the Hanle effect. This result agrees with the fact that the

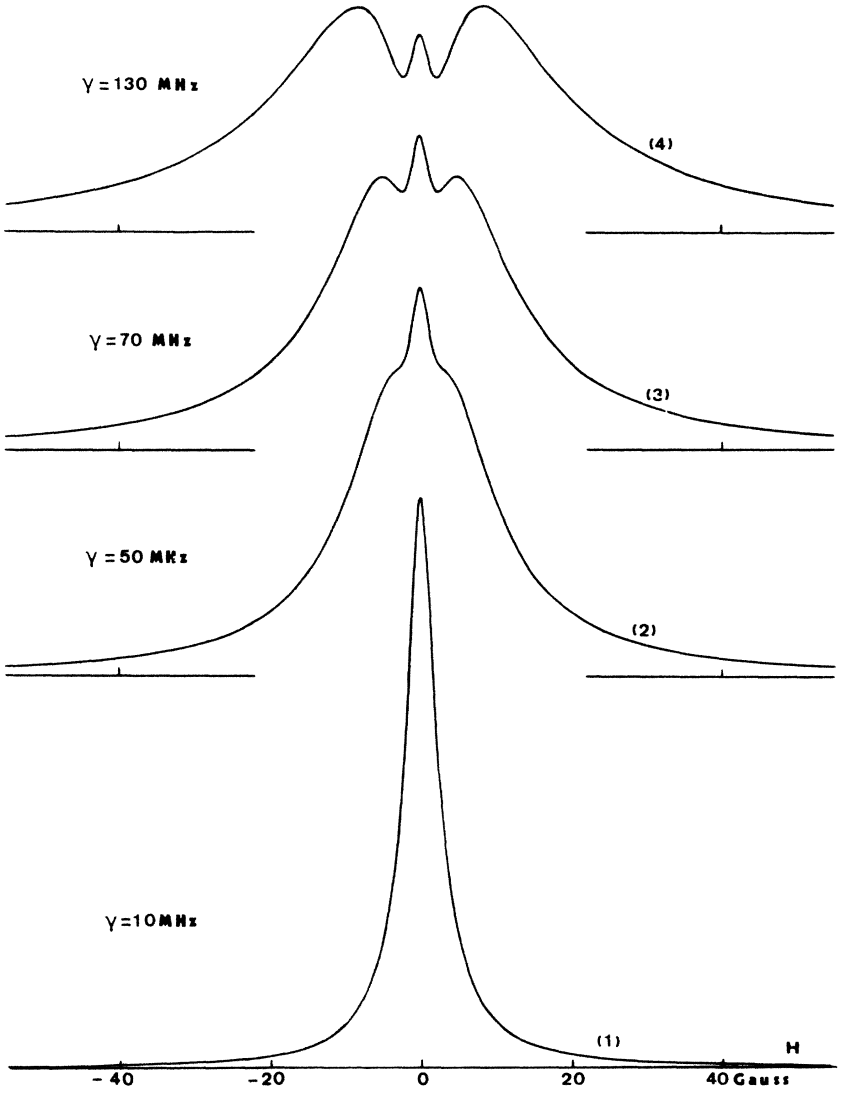

FIG. 11. Shape of the b Hanle effect, for different values of the pumping rate [$J_b = 1 - J_a = 2$ transition; conditions of note (Ref. 16)]. The vertical scale is the same for the different curves. The zero-field alignment of b, ${}_b\rho_2^2(0)$, is maximum for $\gamma = 13.2$ MHz, and vanishes at high laser intensities (see Fig. 6). This explains why the Hanle effect amplitude decreases with increasing γ.

experiments have always shown a Lorentzian shape for the Hanle effect of a $J=2$ level optically pumped by means of a $J=1$-$J=2$ transition (see Refs. 8, 9, and 17 for the 6328-Å and 1.15-μ neon transitions). Nevertheless, the couplings induce a change in the Hanle-effect width. The power broadening is reduced, and the apparent relaxation rate of the transverse alignment, $\Gamma_a^I(2)$, such as obtained from the exact solution, is smaller than the one deduced when the couplings are neglected, $\gamma_a^I(2)$ (see dashed curve of Fig. 7).[21]

b. Hanle effect of b. The results of the computer calculation are shown in Fig. 11. At very low laser intensities, the couplings are vanishing, and the Hanle effect approximately has a Lorentzian shape (curve 1, $\gamma=10$ MHz). When the laser intensity grows, the couplings with ${}_a\rho_2^2$ and ${}_a\rho_4^4$ become important. At first, the ${}_a\rho_4^4$ coupling is the only one visible and implies a narrow central peak on the top of the Hanle effect (curve 2, $\gamma=50$ MHz). The ${}_a\rho_2^2$ coupling cannot be observed because the Hanle effects of levels a and b have nearly the same widths. Afterwards, when the b Hanle effect is more power broadened than the Hanle effect of a, a dip appears because of the ${}_a\rho_2^2$ coupling (curve 3, $\gamma=70$ MHz). The dip becomes deeper and deeper with increasing laser intensities (curve 4, $\gamma=130$ MHz). This behavior of the Hanle-effect shape has been observed in recent experiments.[22]

C. Saturation resonances: Anomalous behavior of the $J_a=2\rightarrow J_f=2$ π-polarized fluorescence

Using (18) and (76), we obtain the following expressions for the longitudinal components of the density matrix:

$$\Gamma_b(0)\,{}_b\rho_0^0 = -\frac{\sqrt{5}}{\sqrt{3}}\,\Gamma_a^*(0)\,{}_a\rho_0^0 = \frac{2\gamma}{3\Delta}\left(-\frac{n}{\sqrt{3}}\,\xi^0+\frac{\xi_b^{20}}{10\sqrt{3}}\,{}_bR_2^2 - \frac{\sqrt{7}}{10}\,\xi_a^{20}\,{}_aR_2^2-\frac{3}{2\sqrt{21}}\,\xi_a^{40}\,{}_aR_2^4\right), \tag{95a}$$

$$\Gamma_b(2)\,{}_b\rho_0^2 = \frac{\gamma\sqrt{2}}{30\Delta}\left(-\frac{n}{\sqrt{3}}\,\xi_b^2+\frac{\xi_{bb}^{22}}{\sqrt{3}}\,{}_bR_2^2 + \frac{2\xi_{ab}^{22}}{\sqrt{7}}\,{}_aR_2^2-\frac{6\sqrt{3}}{\sqrt{7}}\,\xi_{ab}^{42}\,{}_aR_2^4\right), \tag{95b}$$

$$\Gamma_a(2)\,{}_a\rho_0^2 = -\frac{\gamma\sqrt{42}}{30\Delta}\left(-\frac{n}{\sqrt{3}}\,\xi_a^2-\frac{2\xi_{ba}^{22}}{7\sqrt{3}}\,{}_bR_2^2 + \frac{3\xi_{aa}^{22}}{7\sqrt{7}}\,{}_aR_2^2-\frac{2\sqrt{3}}{7\sqrt{7}}\,\xi_{aa}^{42}\,{}_aR_2^4\right), \tag{95c}$$

where coefficients ξ are polynomial functions of γ [see Eqs. (A18)–(A20)]. The populations of the levels exhibit resonant variations in zero field which are connected to the real parts of ${}_a\rho_2^2$, ${}_a\rho_2^4$, and ${}_b\rho_2^2$. These saturation resonances may be observed on the π fluorescence of the levels. For the b level, the intensity of the fluorescence is given by (65). For level a, the intensity of the fluorescence $a\rightarrow f$ is proportional to

$$L_{af}^{\pi} = {}_a\rho_0^0 + A_f\,{}_a\rho_0^2\sqrt{\tfrac{7}{10}}, \tag{96}$$

where $A_f=-1,1$, or $-\frac{2}{7}$ if $J_f=1,2$, or 3. The variations of the $a\rightarrow f$ fluorescence with the magnetic field are proportional to

$$1-\mathcal{S}_{af}^{b2}\,{}_bL_2^2(H)-\mathcal{S}_{af}^{a2}\,{}_aL_2^2(H)-\mathcal{S}_{af}^{a4}\,{}_aL_2^4(H),$$

where ${}_\beta L_2^k(H)$ is the "normalized Hanle effect" [Eq. (27)] and coefficients $\mathcal{S}$ are determined with the help of the zero-field components [(72)–(74)]:

$$\mathcal{S}_{af}^{b2} = \frac{\gamma}{300\Gamma_b(2)}\,\frac{\xi_b^{20}-A_f[\Gamma_a^*(0)/\Gamma_a(2)]\xi_{ba}^{22}}{\xi^0+\frac{7}{20}A_f[\Gamma_a^*(0)/\Gamma_a(2)]\,\xi_a^2} \times\frac{1+\frac{8}{35}\gamma[1/\Gamma_a(4)-1/\Gamma_a(2)]}{\Delta_0}, \tag{97a}$$

$$\mathcal{S}_{af}^{a2} = \frac{7\gamma}{100\Gamma_a^*(2)}\,\frac{\xi_a^{20}-\frac{3}{14}A_f[\Gamma_a^*(0)/\Gamma_a(2)]\xi_{aa}^{22}}{\xi^0+\frac{7}{20}A_f[\Gamma_a^*(0)/\Gamma_a(2)]\xi_a^2} \times\frac{1+\frac{8}{35}\gamma\{1/\Gamma_a(4)+1/[\Gamma_b(2)-\frac{1}{10}\gamma_{bg}]\}}{\Delta_0}, \tag{97b}$$

$$\mathcal{S}_{af}^{a4} = -\frac{2\gamma}{700\Gamma_a(4)}\,\frac{\xi_a^{40}+\frac{1}{5}A_f[\Gamma_a^*(0)/\Gamma_a(2)]\xi_{aa}^{42}}{\xi^0+\frac{7}{20}A_f[\Gamma_a^*(0)/\Gamma_a(2)]\xi_a^2}\,\frac{\tau_3^{-1}\gamma}{\Delta_0}. \tag{97c}$$

$\mathcal{S}_{af}^{\beta k}$ gives the amplitude of the ${}_\beta R_2^k$ contribution to the saturation resonance, relative to the laser-induced change of the fluorescence in strong mag-

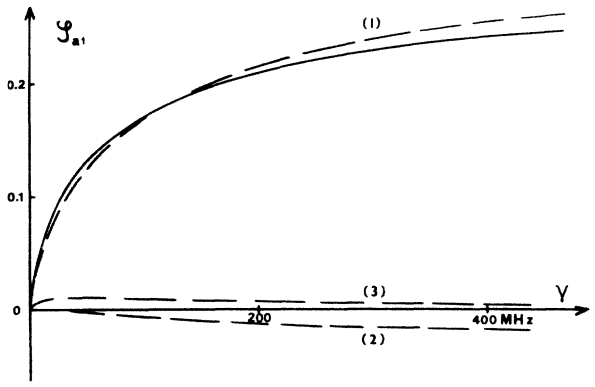

FIG. 12. Amplitude of the saturation resonance on the $J_a=2\rightarrow J_f=1$ fluorescent line for a $J_b=1$-$J_a=2$ laser transition [conditions of note (Ref. 16)]. The continuous curve gives the total amplitude. The dashed curves represent the relative contributions of ${}_a\rho_2^2$ (curve 1), ${}_a\rho_2^4$ (curve 2), and ${}_b\rho_2^2$ (curve 3).

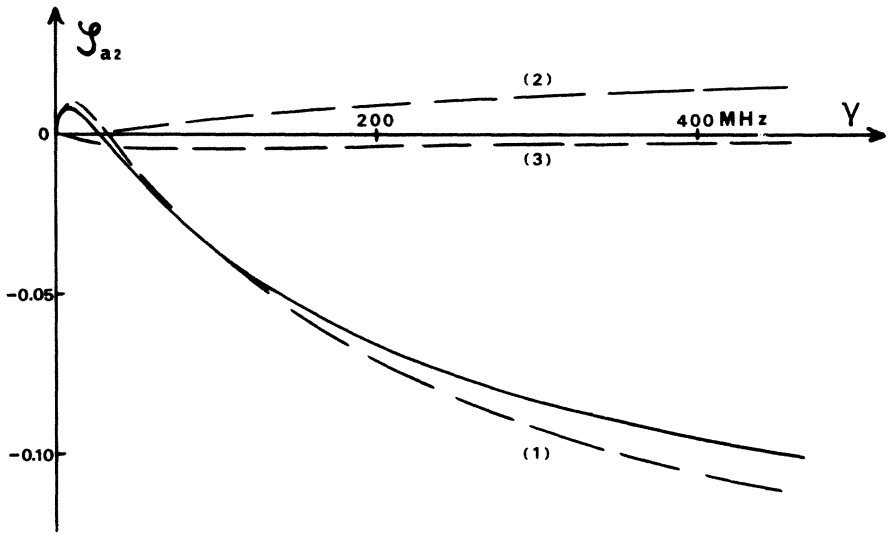

FIG. 13. Amplitude of the saturation resonance on the $J_a = 2 \rightarrow J_f = 2$ fluorescent line (same notations as those of Fig. 12).

netic field. The total amplitude of the saturation resonance is

$$\mathcal{S}_{af} = \mathcal{S}_{af}^{b2} + \mathcal{S}_{af}^{a2} + \mathcal{S}_{af}^{a4}. \tag{98}$$

When $\mathcal{S}_{af}$ is positive, the saturation resonance is in the opposite direction to the laser-induced change of the fluorescence and reduces it in zero field. This is the result obtained for the laser-induced fluorescence, in the case of a $J_b = 1 \text{-} J_a = 0$ or a $J_b = 1 \text{-} J_a = 1$ laser pumping. Here, it is also verified for the $J_a = 2 \rightarrow J_f = 1$ fluorescence. As it is shown in Fig. 12, $\mathcal{S}_{a1}$ is always positive (solid curve). The dashed curves 1, 2, and 3 give the relative contributions of ${}_aR_2^2$, ${}_aR_2^4$, and ${}_bR_2^2$, respectively. Since the alignment of level a is much larger than the alignment of level b and the hexadecapole moment of level a, ${}_aR_2^2$ provides the leading contribution, and the saturation resonance practically has the same shape as the Hanle effect of a.

${}_aR_2^2$ also provides the leading contribution to the saturation resonance of the $J_a = 2 \rightarrow J_f = 2$ fluorescence (Fig. 13). However $\mathcal{S}_{a2}$ exhibits a curious behavior as a function of the laser intensity. $\mathcal{S}_{a2}$, which is positive at weak laser intensities, becomes negative when the laser intensity grows. We obtain the surprising result that the saturation resonance *increases* the laser-induced change of the $J_a = 2 \rightarrow J_f = 2$ fluorescence in zero magnetic field. This anomalous behavior of the saturation has been experimentally observed on the 6328 Å and 1.15-μ neon laser lines.[23] We shall see in Sec. V D, that this anomaly, which is due to higher-order nonlinear effects, is closely connected

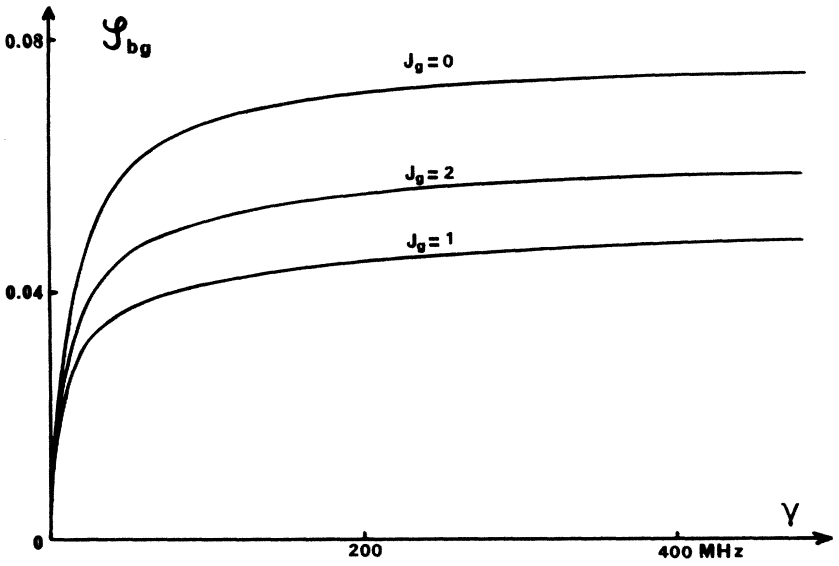

FIG. 14. Amplitude of the saturation resonance on the fluorescence from level b [conditions of note (Ref. 16)].

to the transit time of the atom in the b level.

For the $J_a = 2 \rightarrow J_f = 3$ fluorescence line and for the fluorescence emitted from the b level ($J_b = 1 \rightarrow J_g = 0, 1,$ or 2), the behavior of the saturation resonance is similar to that of the $J_a = 2 \rightarrow J_f = 1$ fluorescence; δ is also positive and the shape of the resonance is practically the same as that of the Hanle effect of a. However, the saturation amplitude is rather smaller for these lines than for the $J_a = 2 \rightarrow J_f = 1$ line (see Fig. 14).[24,25]

D. Two-relaxation-times model

When there is one relaxation rate for every level [$\Gamma_\beta(k) = \gamma_\beta$] and no spontaneous emission ($\gamma_{ba} = 0$), the equations may be simplified. In this case, the set of transitions represented in Fig. 8 by continuous lines is not coupled to the set of dashed lines, and each set may be solved separately.

1. *Hanle effects*

The coherence between the $m_a = \pm 1$ sublevels is given by

$$ {}_a\rho_{1,-1} = (\sqrt{3}\,{}_a\rho_2^2 - 2\,{}_a\rho_2^4)/\sqrt{7}\,. \tag{99}$$

(We define the Zeeman coherence between sublevels m and m' by the usual notation $\rho_{mm'}$).

The equation of motion of ${}_a\rho_{1,-1}$ is deduced from (77a) and (77c). Using the symmetry relations of the χ coefficients [Appendix A, Eqs. (21)–(23)], we obtain

$$ (\gamma_a + \tfrac{1}{10}\gamma + 2i\omega_a)\,{}_a\rho_{1,-1} = -\tfrac{1}{10}n\gamma\chi_a + \tfrac{1}{10}\gamma(1-\chi_a)\,{}_aR_{1,-1}\,, \tag{100}$$

where ${}_aR_{1,-1}$ is the real part of ${}_a\rho_{1,-1}$.

As it was evident in Fig. 8, ${}_a\rho_{1,-1}$, which is connected to the set of dashed lines only, is not coupled to the other Zeeman coherences. The coupling diagram is similar to that of a $J = 1 \text{-} J = 0$ transition, and, subsequently, ${}_aR_{1,-1}$ exhibits Lorentzian variations with the magnetic field. Introducing the mean coherence between the $m_a = 0$ and $m_a = \pm 2$ sublevels,

$$ {}_a\rho_2 = \frac{1}{\sqrt{2}}\,({}_a\rho_{0,-2} + {}_a\rho_{2,0}) = \frac{2\,{}_a\rho_2^2 + \sqrt{3}\,{}_a\rho_2^4}{\sqrt{7}}\,, \tag{101}$$

we find the following equations of motion for the Zeeman coherences coupled by the continuous lines of Fig. 8:

$$ \left(\gamma_a + \frac{2\gamma}{15} + 2i\omega_a\right){}_a\rho_2 - \frac{\gamma}{5\sqrt{3}}\,{}_b\rho_2^2 - \frac{\gamma}{10\sqrt{3}}\,{}_a\rho_4^4 = -\frac{n\gamma}{5\sqrt{3}}\,\chi_a' + \frac{7\gamma}{60}\,(1-\chi_{aa}')\,{}_aR_2 - \frac{\gamma}{10\sqrt{3}}\,(1-\chi_{ba})\,{}_bR_2^2\,, \tag{102a}$$

$$ -\frac{\gamma}{5\sqrt{3}}\,{}_a\rho_2 + \left(\gamma_b + \frac{7\gamma}{30} + 2i\omega_b\right){}_b\rho_2^2 + \frac{\gamma}{5}\,{}_a\rho_4^4 = \frac{n\gamma}{30}\,\chi_b^2 - \frac{\gamma}{10\sqrt{3}}\,(1-\chi_{ab})\,{}_aR_2 + \frac{\gamma}{30}\,(1-\chi_{bb}^{22})\,{}_bR_2^2\,, \tag{102b}$$

$$ -\frac{\gamma}{10\sqrt{3}}\,{}_a\rho_2 + \frac{\gamma}{5}\,{}_b\rho_2^2 + \left(\gamma_a + \frac{\gamma}{5} + 4i\omega_a\right){}_a\rho_4^4 = 0\,, \tag{102c}$$

where coefficients χ are defined by (A22). The equations of motion are reduced to a set of three equations, but it is not much easier to find the solution of (102) than that of (77). The only interest of (102) lies in its straightforward physical interpretation, since ${}_a\rho_2$, ${}_b\rho_2^2$, and ${}_a\rho_4^4$ are associated with clearly defined Zeeman coherences: ${}_a\rho_2$ with the coherence between the $m_a = 0$ and $m_a = \pm 2$ sublevels, ${}_b\rho_2^2$ with the coherence between the $m_b = \pm 1$ sublevels, and ${}_a\rho_4^4$ with the coherence between the $m_a = \pm 2$ sublevels. Then each coupling term of (102) is straightforwardly associated with some of the transitions represented by continuous lines on Fig. 8. For instance, two simultaneous σ^+ (or σ^-) transitions involve a coupling between the $\Delta m = 2$ coherences of levels a and b (${}_a\rho_2 \rightleftharpoons {}_b\rho_2^2$), and so on.

2. *Saturation resonances*

For the π fluorescence emitted from the b level, elementary arguments lead to simplifying the results. For instance, the intensity of the π component of the $J_b = 1 \text{-} J_g = 0$ fluorescence is proportional to the population of the $m_b = 0$ sublevel. Since this sublevel is coupled to the $m_a = \pm 1$ sublevels only (dashed lines of Fig. 8), the saturation resonance is associated with the coherence between these sublevels. Indeed, using (65), (95), and the symmetry relations of coefficients ξ (A24), we show easily that the intensity of this fluorescent line, ${}_b\rho_0^0 - {}_b\rho_0^2\sqrt{2}$, is proportional to $n + {}_aR_{1,-1}(H)$. Then the saturation resonance has the same Lorentzian shape as ${}_aR_{1,-1}$. On the other hand, the intensity of the $J_b = 1 \rightarrow J_g = 1$ fluorescence, ${}_b\rho_0^0 + {}_b\rho_0^2/\sqrt{2}$, is proportional to the population of the $m_b = \pm 1$ sublevels, and subsequently is coupled, by the continuous lines of Fig. 8, to the Zeeman coherence of b (${}_bR_2^2$) and to the Zeeman coherence between the $m_a = 0$ and $m_a = \pm 2$ sublevels of a (${}_aR_2$). For the fluorescence from level a, these kinds of arguments are no longer possible, and every saturation resonance is associated with all the $\Delta m = 2$ Zeeman coherences, ${}_aR_{1,-1}$, ${}_aR_2$, and ${}_bR_2^2$.

In order to determine the physical origin of the anomalous behavior of the saturation of the $J_a = 2 \rightarrow J_f = 2$ fluorescence, we have looked for what happens with this anomalous behavior in the two-

relaxation-times model. Figure 15 shows the variations of the amplitude of the saturation resonance, S_{a2}, as a function of γ/γ_a, for different values of ratio γ_b/γ_a. The zero laser intensity slope of the curves $(11\gamma/270\gamma_a)$ represents the S value such as obtained from the fourth-order perturbation calculation. At high intensities, the asymptotic value of S_{a2} is positive or negative accordingly as γ_b/γ_a is higher or smaller than $\frac{1}{4}(\sqrt{41}-1)\simeq 1.35$. Subsequently, two cases are possible:

(i) If γ_b is higher than $1.35\gamma_a$, S_{a2} keeps the sign of the fourth-order contribution, independent of the laser intensity; the zero-field saturation resonance always reduces the laser-induced change of the fluorescence intensity.

(ii) If γ_b is smaller than $1.35\gamma_a$, S_{a2}, positive at weak laser intensities, becomes negative when the laser intensity grows. This reversal of the saturation resonance increases with decreasing γ_b/γ_a ratios. Subsequently, the anomalous behavior of the saturation seems to be closely connected to the mean lifetime of the b level, i.e., to the transit time of the atom in this level.

This effect may be interpreted by using the diagram of Fig. 8 and pointing out that the population of the $m_a=\pm 2$ sublevels plays a leading part in the intensity of the $J_a=2\rightarrow J_f=2$ fluorescence. Indeed the $m_a=2\rightarrow m_f=2$ transition is 4 times more probable than the $m_a=1\rightarrow m_f=1$ transition, and the $m_a=0\rightarrow m_f=0$ transition is forbidden.

Let us analyze the processes leading to the saturation resonance in the $m_a=2$ sublevel. The stimulated emission of a σ-polarized photon by an atom in the $m_b=1$ sublevel creates coherence between sublevels $m_a=0$ and $m_a=2$ (second-order contribution in a perturbation expansion in the laser field). A new interaction with the laser (now a photon absorption) couples this coherence with the populations of sublevels $m_a=0$, $m_b=1$, and $m_a=2$, and

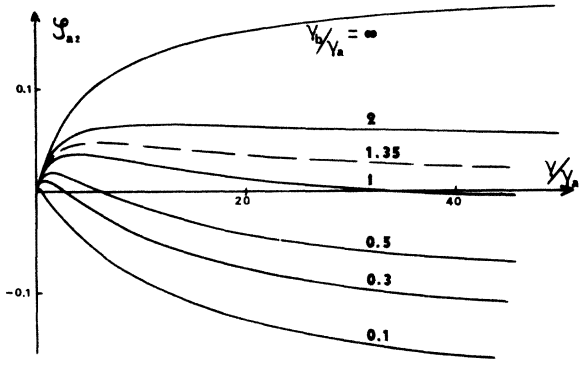

FIG. 15. Amplitude of the saturation resonance on the $J_a=2\rightarrow J_f=2$ fluorescent line, for various ratios of the relaxation rates ($J_b=1$-$J_a=2$ transition; model with two relaxation rates γ_a and γ_b).

produces in these sublevels a saturation resonance which reduces, in zero magnetic field, the laser-induced populations changes (fourth-order term). To the sixth order, the stimulated emission of a σ^- laser photon brings back a part of the $m_b=1$ population into the $m_a=2$ sublevel. Since the laser-induced populations changes of these two sublevels are reversed, the latter process sets the saturation resonance of sublevel $m_b=1$ over against that of $m_a=2$ and *tends to an increasing of the zero-field population change of* $m_a=2$. This effect is important because the $m_b=1\rightarrow m_a=2$ transition is 6 times more probable than the $m_b=1\rightarrow m_a=0$ transition. On the other hand, this effect increases when the laser intensity is strong, and when the population lifetime of level b becomes longer than that of level a (then, the contribution of the $m_b=1$ population grows relatively to that of $m_a=2$).

These considerations explain the behavior of S_{a2} such as shown by Fig. 15. Such a behavior has been experimentally observed.[23] The other sublevels do not exhibit the same behavior as that of $m_a=2$, because of the weak values of the involved transition probabilities. Subsequently, the other fluorescence lines from levels b and a do not show the same anomalous character as the one of the $J_a=2\rightarrow J_f=2$ line, since the $m_a=\pm 2$ sublevels do not bring a leading contribution to these lines any more.

VI. CONCLUSION

In this article, we have analyzed the laser pumping of atoms by means of a nonperturbative method, valid at arbitrary laser intensities. The principal predictions are the following:

(1) For a $J_b=1$-$J_a=0$ transition, the Hanle effect of b always keeps a Lorentzian shape and the populations of the levels exhibit a zero-field saturation resonance proportional to the Hanle effect.

(2) For a $J_b=1$-$J_a=1$ transition, the Hanle effects of both levels also have a Lorentzian shape with a good approximation, and their power broadenings are similar. The saturation resonances come from both the Hanle effects of a and b.

(3) For a $J_b=1$-$J_a=2$ transition, while the Hanle effect of level a is Lorentzian for all the obtainable laser intensities, the one of level b presents a departure from the Lorentzian shape which is due to the couplings with the quadrupole and hexadecapole moments of level a. The saturation resonances come mainly from the Hanle effect of a. The amplitude of the saturation resonance of the $J_a=2\rightarrow J_f=2$ fluorescence exhibits an anomalous behavior because of higher-order effects.

Most of these theoretical predictions have been experimentally observed. A comprehensive study of the experimental verifications will be presented in a forthcoming paper.

The comparison of the exact theory with the fourth-order perturbation calculation[1,26] shows that, for $J=1\text{-}J=0$ and $J=1\text{-}J=1$ transitions, the perturbation calculation deviates from the exact one in a quantitative way only. The physical phenomena are the same in the two theories. For a $J=1\text{-}J=2$ transition, the differences are much more spectacular because of the existence of typically higher-order effects (sixth order and more), in particular the creation of high-order multipole moments in the excited levels. This latter effect is one of the most interesting features of the optical pumping using a laser source. Decomps and Dumont[8,9] have shown that the study of the atomic linear response leads to the determination of the relaxation rates of the population, $\Gamma(0)$, and of the alignment $\Gamma(2)$ of excited levels having a nonzero angular momentum. In the particular case of a $J=1\text{-}J=1$ transition, all the atomic parameters can be deduced from the linear response (obtained by extrapolation at zero laser intensity). Then the experimental fit of the nonlinear effects only implies the determination of the pumping rate γ. On the other hand, the analysis of the nonlinear effects in a $J=1\text{-}J=0$ transition must lead to the measurement of the relaxation rate of the population of the $J=0$ level. This kind of measurement is interesting, but there are other experimental methods (for instance, the study of the level decay by the delayed coincidence method[27]). More original is the possibility of measuring the hexadecapole relaxation rate from an analysis of the nonlinear effects in a $J=1\text{-}J=2$ transition. Pressure broadening of this relaxation rate and subsequent measurements of the collisions cross section are of interest for the study of the multipole expansion of the interaction involved in depolarizing atomic collisions.

APPENDIX

Notations for the $J=1\text{-}J=2$ transition

In Sec. V, we use the following quantities which have the dimension of a time:

$$\tau(0)=\frac{1}{\Gamma_b(0)}+\frac{3}{5\Gamma_a(0)}-\frac{3\gamma_{ba}}{5\Gamma_a(0)\Gamma_b(0)}, \tag{A1}$$

$$\tau(4)=\frac{1}{\Gamma_a(4)}, \tag{A2}$$

$$\tau(p,q,r)=\frac{p}{\Gamma_b(2)}+\frac{q}{\Gamma_a(2)}-\frac{r}{10}\frac{\gamma_{ba}}{\Gamma_a(2)\Gamma_b(2)}, \tag{A3}$$

where p, q, and r are any real numbers. We also introduce matrix τ_j^i $(i,j=1,2,3)$ with the help of particular $\tau(p,q,r)$;

$$(\tau_j^i)=\begin{pmatrix} \tau(\frac{1}{21},1,1) & \tau(\frac{1}{7},1,3) & \tau(1,1,21) \\ \tau(\frac{1}{7},1,1) & \tau(\frac{3}{7},1,3) & \tau(1,\frac{1}{3},7) \\ \tau(1,1,1) & \tau(1,\frac{1}{3},1) & \tau(1,\frac{1}{21},1) \end{pmatrix}, \tag{A4}$$

where i is the column index and j the row index. Matrix M_0 [Eq. (10)] is given by

$$M_0=\begin{pmatrix} 1+\frac{2}{9}\tau(0)\gamma+\frac{7}{75}\tau_1^1\gamma & -\frac{1}{75}\sqrt{6}\,\tau_1^3\gamma \\ -\frac{1}{75}\sqrt{6}\,\tau_3^1\gamma & 1+\frac{6}{25}\tau_3^3\gamma+\frac{8}{35}\tau(4)\gamma \end{pmatrix}, \tag{A5}$$

and its determinant by

$$\Delta_0=1+\gamma\left(\frac{2\tau(0)}{9}+\frac{7\tau_1^1}{75}+\frac{6\tau_3^3}{25}+\frac{8\tau(4)}{35}\right)+\frac{4\gamma^2}{75}\left(\tau(0)\tau_3^3+\frac{20}{21}\tau(0)\tau(4)+\frac{2\tau_1^1\tau(4)}{5}+\frac{8}{21\Gamma_a(2)\Gamma_b(2)}\right). \tag{A6}$$

Matrix M [Eq. (22)] is given by

$$M=\begin{pmatrix} 1+\frac{2\tau(0)}{9}\gamma+\frac{7\tau_1^1}{300}\gamma & -\frac{7\tau_1^2}{60\sqrt{5}}\gamma & \frac{\tau_1^3}{75}\gamma \\ -\frac{7\tau_2^1}{60\sqrt{5}}\gamma & 1+\frac{7\tau_2^2}{60}\gamma & -\frac{\tau_2^3}{5\sqrt{5}}\gamma \\ \frac{\tau_3^1}{75}\gamma & -\frac{\tau_3^2}{5\sqrt{5}}\gamma & 1+\frac{6\tau(4)}{70}\gamma+\frac{4\tau_3^3}{25}\gamma \end{pmatrix}. \tag{A7}$$

Its determinant is

$$\Delta=1+\gamma\left(\frac{2\tau(0)}{9}+\frac{1}{30}\tau(\tfrac{19}{3},\tfrac{31}{7},16)+\frac{6\tau(4)}{70}\right)+\frac{\gamma^2}{10}\left(\frac{7}{15}\tau(0)\tau(1,\tfrac{29}{49},\tfrac{17}{7})+\frac{4}{21}\tau(0)\tau(4)+\frac{\tau(4)}{25}\tau\left(\frac{23}{21},3,8\right)+\frac{37}{210\Gamma_a(2)\Gamma_b(2)}\right)$$

$$+\frac{\gamma^3}{100}\left(\frac{2}{9}\tau(0)\tau(4)\tau_2^2+\frac{32}{105}\frac{\tau(0)}{\Gamma_a(2)\Gamma_b(2)}+\frac{1}{225}\frac{\tau(4)}{\Gamma_a(2)\Gamma_b(2)}\right). \tag{A8}$$

The inverse of M is μ/Δ, where μ is defined by the following matrix elements, $\mu^{k'l'}$ (k' for the row and l' for the column);

$$\mu^{11}=1+\frac{\gamma}{10}\left(\frac{7\tau_2^2}{6}+\frac{8\tau_3^3}{5}+\frac{6\tau(4)}{7}\right)+\frac{\gamma^2}{100}\left(\tau_2^2\tau(4)+\frac{48}{35\Gamma_a(2)\Gamma_b(2)}\right),$$

$$\mu^{12}=\frac{7\tau_1^2}{60\sqrt{5}}\gamma+\left(\tau_1^2\tau(4)+\frac{32}{21\Gamma_a(2)\Gamma_b(2)}\right)\frac{\gamma^2}{100\sqrt{5}},\quad \mu^{13}=-\frac{\tau_1^3}{75}\gamma+\frac{4\gamma^2}{1500\Gamma_a(2)\Gamma_b(2)},$$

$$\mu^{21}=\frac{7\tau_2^1}{60\sqrt{5}}\gamma+\left(\tau_2^1\tau(4)+\frac{32}{21\Gamma_a(2)\Gamma_b(2)}\right)\frac{\gamma^2}{100\sqrt{5}},$$

$$\mu^{22}=1+\left(\frac{2\tau(0)}{9}+\frac{7\tau_1^1}{300}+\frac{4\tau_3^3}{25}+\frac{6\tau(4)}{70}\right)\gamma+\left(\frac{16}{45}\tau(0)\tau_3^3+\frac{4}{21}\tau(0)\tau(4)+\frac{\tau_1^1\tau(4)}{50}+\frac{32}{945\Gamma_a(2)\Gamma_b(2)}\right)\frac{\gamma^2}{10},$$

$$\mu^{23}=\frac{\tau_2^3}{5\sqrt{5}}\gamma+\frac{2\gamma^2}{45\sqrt{5}}\left(\tau(0)\tau_2^3+\frac{1}{15\Gamma_a(2)\Gamma_b(2)}\right),\quad \mu^{31}=-\frac{\tau_3^1}{75}\gamma+\frac{4\gamma^2}{1500\Gamma_a(2)\Gamma_b(2)},$$

$$\mu^{32}=\frac{\tau_3^2}{5\sqrt{5}}\gamma+\frac{2\gamma^2}{45\sqrt{5}}\left(\tau(0)\tau_3^2+\frac{1}{15\Gamma_a(2)\Gamma_b(2)}\right),\quad \mu^{33}=1+\gamma\left(\frac{2\tau(0)}{9}+\frac{7\tau_1^1}{300}+\frac{7\tau_2^2}{60}\right)+\frac{7\gamma^2}{270}\left(\tau(0)\tau_2^2+\frac{1}{50\Gamma_a(2)\Gamma_b(2)}\right). \tag{A9}$$

In the equations of motion of the transverse components, the following coefficients are introduced [Δ is defined by (A8)]:

$$\Delta\chi_a^2=1+\frac{\gamma}{70}[\tau(15,\tfrac{34}{3},\tfrac{23}{60})+6\tau(4)]+\frac{\gamma^2}{30}\left(\tau(4)\tau(\tfrac{1}{7},\tfrac{2}{5},1)+\frac{4}{7\Gamma_a(2)\Gamma_b(2)}\right),$$

$$\Delta\chi_b^2=1+\frac{\gamma}{10}\left(\tau(2,\tfrac{15}{7},6)+\frac{6\tau(4)}{7}\right)+\frac{\gamma^2}{50}\left(\tau(4)\tau(\tfrac{2}{7},1,2)+\frac{12}{7\Gamma_a(2)\Gamma_b(2)}\right),\quad \Delta\chi^4{}_a=\gamma\frac{\tau_3^1}{10}-\frac{\gamma^2}{50\Gamma_a(2)\Gamma_b(2)} \tag{A10}$$

for the source-terms, and

$$\Delta\chi_{aa}^{22}=1+\frac{7\gamma}{230}\left(\frac{166}{63}\tau(0)+\tfrac{1}{3}\tau(\tfrac{425}{21},14,50)+\frac{14}{5}\tau(4)\right)$$
$$+\frac{7\gamma^2}{690}\left(\frac{2}{5}\tau(0)\tau(\tfrac{25}{7},\tfrac{1}{3},5)+\frac{2}{3}\tau(0)\tau(4)+\frac{7}{5}\tau(4)\tau(\tfrac{5}{21},\tfrac{4}{5},2)+\frac{5}{3\Gamma_a(2)\Gamma_b(2)}\right),$$

$$\Delta\chi_{ba}^{22}=1+\frac{\gamma}{10}\left(\frac{13}{9}\tau(0)+\frac{5}{3}\tau(\tfrac{4}{3},\tfrac{4}{5},\tfrac{7}{2})+\frac{4}{5}\tau(4)\right)+\frac{\gamma^2}{100}\left(\frac{10}{3}\tau(0)\tau(1,\tfrac{1}{5},3)+\frac{10}{9}\tau(0)\tau(4)+\frac{7\tau(4)}{15}\tau(\tfrac{10}{21},2,5)+\frac{5}{3\Gamma_a(2)\Gamma_b(2)}\right),$$

$$\Delta\chi_{aa}^{42}=1+\frac{7\gamma}{30}\left(\frac{20}{21}\tau(0)+\tau(\tfrac{55}{21},1,10)\right)+\frac{7\gamma^2}{30}\left(\tau(0)\tau(\tfrac{5}{7},\tfrac{1}{3},5)+\frac{1}{6\Gamma_a(2)\Gamma_b(2)}\right),$$

$$\Delta\chi_{ab}^{22}=1+\frac{\gamma}{10}\left(\frac{13}{9}\tau(0)+\frac{2}{3}\tau(\tfrac{10}{3},2,7)+\frac{4}{5}\tau(4)\right)+\frac{\gamma^2}{100}\left(\frac{2}{3}\tau(0)\tau(5,1,7)+\frac{10}{9}\tau(0)\tau(4)+\frac{7\tau(4)}{15}\tau(\tfrac{10}{21},2,4)+\frac{5}{3\Gamma_a(2)\Gamma_b(2)}\right),$$

$$\Delta\chi_{bb}^{22}=1+\frac{\gamma}{10}\left(2\tau(0)+\tau(2,\tfrac{9}{7},6)+\frac{18}{35}\tau(4)\right)+\frac{\gamma^2}{100}\left(4\tau(0)\tau(1,\tfrac{3}{7},3)+\frac{20}{21}\tau(0)\tau(4)+\frac{2}{5}\tau(4)\tau(\tfrac{4}{21},1,2)+\frac{6}{7\Gamma_a(2)\Gamma_b(2)}\right),$$

$$\Delta\chi_{ab}^{42}=1+\frac{\gamma}{9}[2\tau(0)+\tau(\tfrac{13}{10},\tfrac{3}{2},\tfrac{42}{5})]+\frac{\gamma^2}{30}\left(\tau(0)\tau(1,1,7)+\frac{1}{10\Gamma_a(2)\Gamma_b(2)}\right),$$

$$\Delta\chi_{aa}^{24}=1+\frac{7\gamma}{30}\left(\frac{20}{21}\tau(0)+\tau(\tfrac{55}{21},1,4)\right)+\frac{7\gamma^2}{30}\left(\tau(0)\tau(\tfrac{5}{7},\tfrac{1}{3},1)+\frac{1}{6\Gamma_a(2)\Gamma_b(2)}\right),$$

$$\Delta\chi_{ba}^{24}=1+\frac{\gamma}{9}[2\tau(0)+\tau(\tfrac{13}{10},\tfrac{3}{2},\tfrac{21}{5})]+\frac{\gamma^2}{30}\left(\tau(0)\tau(1,1,3)+\frac{1}{10\Gamma_a(2)\Gamma_b(2)}\right),$$

$$\Delta\chi_{aa}^{44}=1+\frac{7\gamma}{150}\left(\frac{100}{21}\tau(0)+\tau(\tfrac{23}{21},3,8)\right)+\frac{7\gamma^2}{270}\left(\tau(0)\tau_2^2+\frac{1}{50\Gamma_a(2)\Gamma_b(2)}\right) \tag{A11}$$

for the coupling terms. The equations of motion of the transverse components of the density matrix may be written in a compact shape,

$$(\Gamma+i\Omega)\rho=n\Lambda+\chi R, \tag{A12}$$

if we introduce the 4×4 matrices

$$\Gamma=\begin{pmatrix} \Gamma_a(2)+\frac{5\gamma}{42} & -\left(\frac{2\gamma}{5\sqrt{21}}+\frac{\sqrt{21}}{10}\gamma_{ba}\right) & \frac{\gamma}{35\sqrt{3}} & -\frac{\gamma}{5\sqrt{21}} \\ -\frac{2\gamma}{5\sqrt{21}} & \Gamma_b(2)+\frac{7\gamma}{30} & -\frac{\gamma}{5\sqrt{7}} & \frac{\gamma}{5} \\ \frac{\gamma}{35\sqrt{3}} & -\frac{\gamma}{5\sqrt{7}} & \Gamma_a(4)+\frac{4\gamma}{35} & -\frac{\gamma}{10\sqrt{7}} \\ -\frac{\gamma}{5\sqrt{21}} & \frac{\gamma}{5} & -\frac{\gamma}{10\sqrt{7}} & \Gamma_a(4)+\frac{\gamma}{5} \end{pmatrix}, \tag{A13}$$

$$\Omega=2\begin{pmatrix} \omega_a & 0 & 0 & 0 \\ 0 & \omega_b & 0 & 0 \\ 0 & 0 & \omega_a & 0 \\ 0 & 0 & 0 & 2\omega_a \end{pmatrix}, \tag{A14}$$

$$\chi=\gamma\begin{pmatrix} \frac{23}{210}(1-\chi_{aa}^{22}) & -\frac{1}{5\sqrt{21}}(1-\chi_{ba}^{22}) & \frac{1}{70\sqrt{3}}(1-\chi_{aa}^{42}) & 0 \\ -\frac{1}{5\sqrt{21}}(1-\chi_{ab}^{22}) & \frac{1}{30}(1-\chi_{bb}^{22}) & -\frac{1}{10\sqrt{7}}(1-\chi_{ab}^{42}) & 0 \\ \frac{1}{70\sqrt{3}}(1-\chi_{aa}^{24}) & -\frac{1}{10\sqrt{7}}(1-\chi_{ba}^{24}) & \frac{3}{28}(1-\chi_{aa}^{44}) & 0 \\ 0 & 0 & 0 & 0 \end{pmatrix}, \tag{A15}$$

and the column vectors

$$\Lambda=\frac{\gamma}{30}\begin{pmatrix} -\sqrt{21}\chi_a^2 \\ \chi_b^2 \\ \frac{2}{\sqrt{7}}\chi_a^4 \\ 0 \end{pmatrix}, \tag{A16}$$

$$\rho=\begin{pmatrix} {}_a\rho_2^2 \\ {}_b\rho_2^2 \\ {}_a\rho_2^4 \\ {}_a\rho_4^4 \end{pmatrix}. \tag{A17}$$

R is the real part of ρ. The following coefficients are used in the saturation resonances of the populations:

$$\begin{aligned} &\xi^0=\mu^{11}\quad \xi_a^{40}=\mu^{13}, \\ &\xi_b^{20}=1+\frac{\gamma}{10}\left(\tau(2,\tfrac{15}{7},3)+\frac{6}{7}\tau(4)\right) \\ &\qquad+\frac{\gamma^2}{100}\left(\tau(\tfrac{4}{7},2,6)\tau(4)+\frac{24}{7\Gamma_a(2)\Gamma_b(2)}\right), \\ &\xi_a^{20}=1+\frac{\gamma}{10}\left(\tau(\tfrac{15}{7},\tfrac{34}{21},6)+\frac{6}{7}\tau(4)\right) \\ &\qquad+\frac{\gamma^2}{100}\left(\tau(\tfrac{10}{21},\tfrac{4}{3},4)\tau(4)+\frac{40}{21\Gamma_a(2)\Gamma_b(2)}\right), \end{aligned} \tag{A18}$$

$$\begin{aligned} &\xi_b^2=1-\frac{3\gamma}{70}\left(\frac{9}{\Gamma_a(2)}-\frac{2}{\Gamma_a(4)}\right)-\frac{\gamma^2}{50\Gamma_a(2)\Gamma_a(4)}, \\ &\xi_{bb}^{22}=1+\frac{\gamma}{10}\left(2\tau(0)+\frac{3}{\Gamma_a(2)}-\frac{6}{5\Gamma_a(4)}\right)+\frac{\gamma^2}{10}\left(\frac{24\tau(0)}{35\Gamma_a(2)}-\frac{2\tau(0)}{7\Gamma_a(4)}-\frac{2}{50\Gamma_a(2)\Gamma_a(4)}\right), \\ &\xi_{ab}^{22}=1+\frac{\gamma}{10}\left(3\tau(0)+\frac{1}{3\Gamma_a(2)}+\frac{6}{5\Gamma_a(4)}\right)+\frac{\gamma^2}{10}\left(-\frac{4\tau(0)}{15\Gamma_a(2)}+\frac{\tau(0)}{3\Gamma_a(4)}+\frac{7}{75\Gamma_a(2)\Gamma_a(4)}\right), \\ &\xi_{ab}^{42}=1+\frac{\gamma}{9}\left(2\tau(0)+\frac{11}{10\Gamma_a(2)}\right)+\frac{\gamma^2}{45}\frac{\tau(0)}{\Gamma_a(2)}, \end{aligned} \tag{A19}$$

and

$$\xi_a^2 = 1 - \frac{\gamma_{ba}}{10\Gamma_b(2)} + \frac{\gamma}{70}\left[\frac{13}{\Gamma_b(2)} + \frac{6}{\Gamma_a(4)}\left(1 - \frac{\gamma_{ba}}{10\Gamma_b(2)}\right)\right] + \frac{\gamma^2}{350\Gamma_b(2)\Gamma_a(4)},$$

$$\xi_{ba}^{22} = 1 + \frac{7\gamma_{ba}}{20\Gamma_b(2)} + \frac{\gamma}{10}\left[3\tau(0)\left(1 + \frac{7\gamma_{ba}}{30\Gamma_b(2)}\right) + \frac{3}{\Gamma_b(2)} + \frac{6}{5\Gamma_a(4)}\left(1 - \frac{7\gamma_{ba}}{20\Gamma_b(2)}\right)\right]$$
$$+ \frac{\gamma^2}{10}\left[\frac{4\tau(0)}{5\Gamma_b(2)} + \frac{\tau(0)}{3\Gamma_a(4)}\left(1 - \frac{3\gamma_{ba}}{10\Gamma_b(2)}\right) - \frac{1}{75\Gamma_a(4)\Gamma_b(2)}\right],$$

$$\xi_{aa}^{22} = 1 - \frac{7\gamma_{ba}}{15\Gamma_b(2)} + \frac{\gamma}{30}\left[\frac{158}{9}\tau(0)\left(1 - \frac{189\gamma_{ba}}{790\Gamma_b(2)}\right) + \frac{25}{9\Gamma_b(2)} + \frac{14}{5\Gamma_a(4)}\left(1 - \frac{3\gamma_{ba}}{5\Gamma_b(2)}\right)\right] \qquad \text{(A20)}$$
$$+ \frac{\gamma^2}{90}\left[\frac{8\tau(0)}{\Gamma_b(2)} + \frac{14\tau(0)}{3\Gamma_a(4)}\left(1 - \frac{3\gamma_{ba}}{10\Gamma_b(2)}\right) - \frac{7}{15\Gamma_b(2)\Gamma_a(4)}\right],$$

$$\xi_{aa}^{42} = 1 - \frac{21\gamma_{ba}}{10\Gamma_b(2)} + \frac{\gamma}{9}\left[2\tau(0)\left(1 - \frac{21\gamma_{ba}}{10\Gamma_b(2)}\right) - \frac{29}{10\Gamma_b(2)}\right] - \frac{\gamma^2}{15}\frac{\tau(0)}{\Gamma_b(2)}.$$

Two-relaxation-times model

For the two-relaxation-times model, the matrix of the χ coefficients is symmetrical

$$\chi_{\alpha\beta}^{kk''} = \chi_{\beta\alpha}^{k''k}. \qquad \text{(A21)}$$

We use the following coefficients for the study of the Zeeman coherence

$$\chi_a = \chi_a^2 + \frac{4}{21}\chi_a^4 = \left[1 + \frac{\gamma}{10}\left(\frac{2}{\gamma_b} + \frac{1}{\gamma_a}\right)\right]^{-1},$$

$$\chi_a' = \chi_a^2 - \frac{\chi_a^4}{7} = \frac{1}{\Delta'}\left(1 + \frac{2\gamma}{15\gamma_a}\right),$$

$$\chi_b^2 = \frac{1}{\Delta'}\left(1 + \frac{\gamma}{5\gamma_a}\right),$$

$$\chi_{aa}' = \frac{46\chi_{aa}^{22} + 3\chi_{aa}^{24}}{49} = \frac{1}{\Delta'}\left[1 + \frac{\gamma}{210}\left(\frac{25}{\gamma_b} + \frac{38}{\gamma_a}\right)\right],$$

$$\chi_{ab} = \chi_{ab}^{22} = \chi_{ab}^{42} = \frac{1}{\Delta'}\left[1 + \frac{\gamma}{30}\left(\frac{5}{\gamma_b} + \frac{6}{\gamma_a}\right)\right], \qquad \text{(A22)}$$

$$\chi_{bb}^{22} = \frac{1}{\Delta'}\left[1 + \frac{\gamma}{5}\left(\frac{1}{\gamma_b} + \frac{1}{\gamma_a}\right)\right],$$

where

$$\Delta' = 1 + \frac{\gamma}{30}\left(\frac{7}{\gamma_b} + \frac{8}{\gamma_a}\right) + \frac{\gamma^2}{150\gamma_a}\left(\frac{3}{\gamma_b} + \frac{2}{\gamma_a}\right). \qquad \text{(A23)}$$

Coefficients ξ [Eq. (A20)] verify the following relations:

$$\xi_b^{20} = \xi_{bb}^{22}$$

and

$$\frac{10\xi^0 - \xi_b^2}{9} = \frac{7\xi_a^{20} + 2\xi_{ab}^{22}}{9} = \xi_{ab}^{42} - \frac{5}{6}\xi_a^{40} = \Delta'. \qquad \text{(A24)}$$

[1] M. Ducloy, Phys. Rev. A 8, 1844 (1973).

[2] W. R. Bennett, Jr., Phys. Rev. 126, 580 (1962).

[3] M. Dumont and B. Decomps, J. Phys. (Paris) 29, 181 (1968).

[4] Let me point out that if either J_a and J_b are equal or the $b \to a$ spontaneous emission is negligible ($\gamma_{ba} = 0$), the M_0 matrix is symmetrical.

[5] In I, I have considered a σ_y polarization. Transposing $0x$ and $0y$ can be made by changing ρ_Q^k into $(-)^{Q/2}\rho_Q^k$.

[6] M. Rotenberg, R. Bivins, N. Metropolis, and J. K. Wooten, Jr., *The 3-j and 6-j symbols* (Crosby Lockwood and Son, Ltd., London, 1959).

[7] A. R. Edmonds, *Angular Momentum in Quantum Mechanics* (Princeton U. P., Princeton, N. J., 1957).

[8] B. Decomps and M. Dumont, J. Phys. (Paris) 29, 443 (1968).

[9] B. Decomps and M. Dumont, IEEE J. Quant. Electron. QE4, 916 (1968).

[10] M. Ducloy, E. Giacobino-Fournier, and B. Decomps, J. Phys. (Paris) 31, 533 (1970).

[11] M. Ducloy, Opt. Commun. 3, 205 (1971).

[12] F. Bloch and A. Siegert, Phys. Rev. 57, 522 (1940).

[13] When γ is lower than $\gamma_0 = 3\Gamma_b(2)/\eta + 1$, δ can be expressed as an infinite series $\delta = [1/(\eta+1)]\sum_{p=0}^{\infty}(-)^p(\gamma/\gamma_0)^{p+1}$. As a matter of fact, this expression gives the result of the usual perturbation theory, when BLA is valid. Then the perturbation development is convergent if $\gamma < \gamma_0$ only. In the case of the 1.52-μ neon line (see Fig. 1), $\gamma_0 = 5.7$ MHz. We shall see, in a forthcoming publication, that the experiments have shown that γ can be as high as 80 MHz. This explains the importance of theories based on nonperturbative methods.

[14] J. Datchary and M. Ducloy, Compt. Rend. 274B, 337 (1972).

[15] J. Datchary, Thèse de Troisième Cycle (University of Paris, 1972) (unpublished); J. Datchary and M. Ducloy (unpublished).

[16] In this section, numerical applications of the theory will be performed using the following values of the relaxation rates (in MHz): $\Gamma_a(0) = 9.8$, $\Gamma_a(2) = \Gamma_a(4) = 14.5$, $\Gamma_b(0) = 2.75$, $\Gamma_b(2) = 5.75$, and $\gamma_{ba} = 0.5$. The Landé

factors are $g_a = 1.299$ and $g_b = 1.293$. This nearly corresponds to the experimental conditions of the 6328-Å neon laser line (transition $3s_2 - 2p_4$), when the neon pressure is equal to 1.5 torr (see Refs. 8 and 9).

[17] B. Decomps, Thesis (University of Paris, 1969) (unpublished).

[18] The Principal difficulty of this measurement consists in the determination of the correspondence between the experimentally measured laser intensity and the pumping rate γ. The best way seems to lie in the analysis of the power broadening of the a Hanle effect (see Fig. 7 and Ref. 21).

[19] However, in zero field, the density matrix may be obtained with the help of Eqs. (72)–(74) and has a simple analytic shape. It is possible to verify that Eqs. (72)–(74) provide the solution of Eqs. (77), but the calculation, which is very complicated, will not be reproduced here.

[20] $\epsilon = -0.10$ when $\gamma = 100$ MHz. The contribution of the ${}_a\rho_2^4$ coupling is weak in comparison with that of ${}_a\rho_2^2$, but this is not negligible relatively to the direct excitation χ_b^2.

[21] The power broadening of the Hanle effect of the a level is not very dependent on the various relaxation rates of the levels. Subsequently the analysis of this power broadening is particularly well convenient for the determination of the pumping rate γ. This is the reason why it is very important to have the exact theoretical variations of the width with the pumping rate. These remarks are also valid for the $J=1$–$J=0$ and $J=1$–$J=1$ transitions.

[22] M. Ducloy, M. P. Gorza, and B. Decomps, Opt. Commun. 8, 21 (1973).

[23] M. P. Gorza, B. Decomps, and M. Ducloy, Opt. Commun. 8, 323 (1973). Parameter δ, which is introduced in this reference, is connected to the pumping rate by the relation $\gamma = 30\delta$.

[24] In the experimental study of the 6328-Å neon line, B. Decomps and M. Dumont (Ref. 8) have introduced the dimensionless quantity $F(a, f, f') = L_{af}^{\pi}/L_{af'}^{\pi}$, which is the ratio of the intensities of two different fluorescent lines emitted from the same level. Particularly, B. Decomps *et al.*, have studied the variations of $F(a,2,1)$ with the laser intensity $F(a,2,1) = (\sqrt{10}\,{}_a\rho_0^0 + \sqrt{7}\,{}_a\rho_0^2)/(\sqrt{10}\,{}_a\rho_0^0 - \sqrt{7}\,{}_a\rho_0^2)$. In zero magnetic field, ${}_a\rho_0^0$ and ${}_a\rho_0^2$ are nearly proportional [Eqs. (72)–(74)]. As it is for the zero-field anisotropy of the fluorescence of level a, $F(H=0)$ is practically independent of the laser intensity. In strong fields [$\omega_\beta \gg \Gamma_\beta(k)$], (95) imply ${}_a\rho_0^2/{}_a\rho_0^0 = [\sqrt{7}/2\sqrt{10}][\Gamma_a^*(0)/\Gamma_a(2)]\xi_a^2/\xi^0$. The numerical application shows that $F(H=\infty)$ decreases with increasing laser intensities. These results are in qualitative agreement with the experiments (Fig. 3 of Ref. 8).

[25] In the case of the 6328-Å neon line, where the Landé factors are nearly equal, all the results obtained in weak field can be extended to the strong field phenomena, when the laser modes are phase locked (see Sec. IV B 2 of article I and, in particular, the equations (I-83) and (I-84). The lateral saturation resonances of the π fluorescence have the same shape as the zero-field saturation resonance. Subsequently for the leading part, they must be ascribed to the Zeeman coherence of the $J_a = 2$ level ($2p_4$, in the case of 6328-Å), whether the fluorescent line is issued from level a or from level b. This result, valid at arbitrary laser intensitites, have been shown by M. Dumont (Ref. 26) for the fourth-order theoretical calculation and have been experimentally verified very well (see Fig. 7 of Ref. 26). Fork, Hargrove, and Pollack, who had observed these lateral resonances [Phys. Rev. Lett. 12, 705 (1964)] had erroneously ascribed them to the $J_b = 1$ level (here, $3s_2$ of neon). They had deduced this from the fact that they did not observe these resonances on the $2p_4$–$1s_5$ fluorescence line ($J_a = 2 \rightarrow J_f = 2$). Indeed, their experimental conditions must have nearly corresponded to the zero point of δ_{a2}, in Fig. 13.

[26] M. Dumont, J. Phys. (Paris) 33, 971 (1972).

[27] J. Z. Klose, Phys. Rev. 141, 181 (1966); W. R. Bennett and P. J. Kindlmann, Phys. Rev. 149, 38 (1966).